Packet Propagation in an Associative Feedforward Network

Department of Complexity Science and Engineering
Graduate School of Frontier Sciences
The University of Tokyo

Kazuya Ishibashi

Abstract

Nervous system is a major information processing center of our body. An important goal of neuroscience research is to clarify the mechanism of its information processing. Many researchers have attempted to clarify the processing done by the neural network. However the neural networks are generally too complex for their activity to be described in detail. To investigate their properties, I constructed and analyzed a simplified feedforward network of a spiking neuron model. For simplicity, I focused on the propagation of transient spikes. It is well known that when a homogeneous feedforward network receives transient input, it transmits stable synchronous spikes called a "pulse packet". Such a network is called a "synfire chain". The network can transmit only one pattern of packets and the packets are the synchronous spikes of all the neurons in one layer. The propagation of pulse packets in inhomogeneous feedforward networks has not been thoroughly investigated yet. In this dissertation I show the associative feedforward network that should be able to send multiple patterns of pulse packets by embedding memory patterns in the synaptic weights.

First, I show that the associative feedforward network can transmit embedded pulse packets as expected. In the analysis, We constructed the network of the leaky integrate-and-fire neuron model. We used the Fokker-Planck equations to describe the properties of the network by using macroscopic parameters. Although activation of one memory pattern results in the propagation of the synchronous activated pattern packet, activation of two patterns temporally splits the propagation into the groups called 'sub-

lattices'. I describe the details of this activity and its mechanism.

Next, I discuss the relationship between the activity and the density of the embedded patterns in terms of the temporal split between sublattices, the basin of the attraction, and the storage capacity. The analysis revealed that sparse coding is better than dense coding for synchronous spike propagation. This implies that sparse coding is better for information processing by the neural networks.

We also analyzed the activity when the embedded patterns are correlated and found that the correlation does not seem to work well for synchronous spike propagation. Moreover, I discuss the relationship between the memory pattern correlation and the pattern rate.

Our analysis of the activity of the associative feedforward network has clarified many of the properties of packets propagation. Our research is a basic study of a network that can transmit multiple patterns of packets.

Preface

This work has been carried out in the Okada Laboratory, Department of Complexity Science and Engineering, Graduate School of Frontier Sciences, The University of Tokyo.

I would like to express my deep gratitude to my advisor, Prof. Masato Okada, for his advice and constant encouragement. I would also like to thank Dr. Kosuke Hamaguchi for his enthusiastic technical advice and valuable discussions.

I would like to thank all past and present members and collaborators of the Okada Laboratory, particularly Dr. Kazuyuki Hara, Dr. Yoichi Miyawaki, Dr. Sei Suzuki, Dr. Toshiaki Omori, Dr. Keiji Miura, Dr. Kazuho Watanabe, Mr. Yukihiro Tsuboshita, Mr. Mitsuhiro Urano, Mr. Kentaro Katahira, Mr. Cousseau Florent, Mr. Masafumi Oizumi, Mr. Hiroyuki Tanaka, Mr. Kensei Yamaji, Mr. Munenori Iida, Mr. Yusuke Usui, Mr. Tomohiro Kubo, Mr. Tatsuhiro Tajima, and Mr. Cho Tatsuya.

I would like to thank Dr. Toshihiko Hosoya and Mr. Toshiyuki Ishii for their support.

I am grateful to the members of my thesis committee: Prof. Mitsuhiro Toriumi, Prof. Akinao Nose, Prof. Seiji Sugita, and Prof. Shigeo Takahashi.

Lastly, let me thank my father, my mother, my brother, and my wife for their invaluable support.

Kazuya Ishibashi

Contents

Chapter 1

Introduction

1.1 Background

Nervous system receives the input from both external and internal environments and outputs motor control signals. One of the goals of neuroscience is to clarify how the nervous system processes the information. In particular, how does it describe, store, transmit, and transform the information? These questions are too broad and neural networks are generally too complex for them to be answered at the same time. To investigate the processing mechanism, we focused on information transmission. Reliable information transmission is necessary for efficient information processing. Understanding the transmission is a non-trivial problem because biological systems are noisy, and the responses of neurons are stochastic (Mainen and Sejnowski, 1995; Gerstner and Kistler, 2002). Consequently, how neural networks transmit information reliably is an important question.

1.2 Synfire chain

"Synfire chain" is an important concept in reliable information transmission. A synfire chain is a functional feedforward network that can transmit synchronous spikes stably (Abeles, 1991). Diesmann *et al.* analyzed the function

of a homogeneous feedforward network as a synfire chain constructed by using a spiking neuron model with white Gaussian noise (Diesmann *et al.*, 1999). They showed that a homogeneous feedforward network has two modes after convergence: a synchronous propagation mode and spontaneous firing mode. Figure 1.1 shows the convergence. The attractor at the upper left represents the synchronous propagation mode, and the flow arrows to the lower right represent the spontaneous firing mode. In synchronous propagation mode, the network stably and reproducibly transmits synchronous spikes, called a "pulse packet". Even though the neurons receive noisy current, the network can transmit a group of spikes reliably with msec precision. However, the network cannot transmit information in spontaneous firing mode. For the synchronous, reproductive and stable properties of spikes and the simplicity of the network, synfire chains have been extensively researched theoretically (Bienenstock, 1995; Câteau and Fukai, 2001; Gewaltig *et al.*, 2001; Kistler and Gerstner, 2002; van Rossum *et al.*, 2002; Li and Greenside, 2006; Jin *et al.*, 2007) and a synfire chain network has been iteratively constructed *in vitro* (Reyes 2003).

A notable feature of the synfire chain is its ability to generate repeated spike patterns with msec precision. The repeated spike patterns have been experimentally observed *in vivo* (Abeles and Gerstin, 1988; Abeles *et al.*, 1993; Prut *et al.*, 1998; Hahnloser *et al.*, 2002; Shmiel *et al.*, 2005; 2006) and *in vitro* (Ikegaya *et al.*, 2005; Mokeichev *et al.*, 2007). Figure 1.2, adapted from Hahnloser *et al.*, 2002, shows that the recording neurons (numbers 1-8) repeatedly generate temporally conserved spike patterns more against the song motif. The homogeneous synfire chain can reproduce repeated spike patterns like this because of its high reproductivity and its temporal accuracy. If one would like to generate more complex song motifs, the network in which multiple synfire chains coexist might be useful.

Another notable feature of the synfire chain is its ability to generate synchronous spikes, which may be important in binding problems (Gray *et*

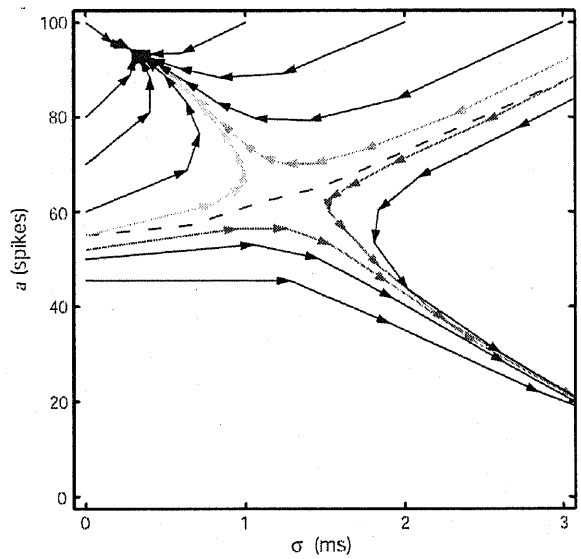

Figure 1.1: Figure adapted from Diesmann *et al.*, 1999. Arrows show the changes in number of spikes a (vertical axis) and degree of synchrony σ (horizontal axis) between layers.

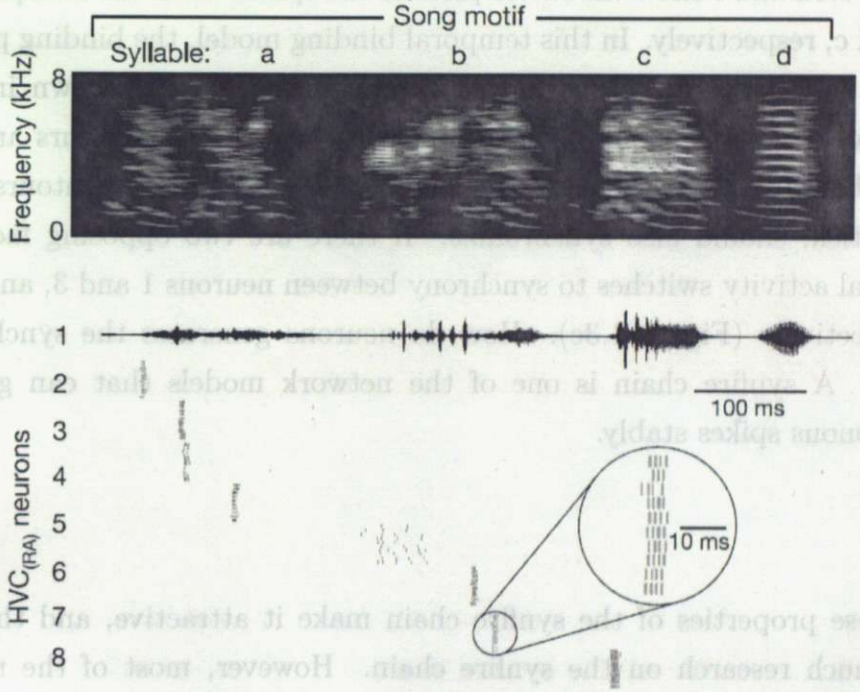

Figure 1.2: Figure adapted from Hahnloser *et al.*, 2002, showing raster plot of neuronal spikes. The upper figure represents the song motif and lower figure represents spikes of 8 RA neurons in HVC.

al., 1989; Gray, 1999; Singer, 1999; Engel *et al.*, 2001). Figure 1.3, adapted from Engel *et al.*, 2001, shows an example of temporal binding model. Figure 1.3a shows bistable images. Bistability means that two interpretations are possible. In this case, one interpretation is that one face is partially occluded by a candlestick (Figure 1.3b); the other is that there are two opposing faces (Figure 1.3c). The lower figure 1.3a shows the receptive fields of four neurons. Figures 1.3d and e show the raster plots of the spikes when the interpretation is b and c, respectively. In this temporal binding model, the binding problem can be solved by exploiting the synchrony of spikes. As shown in figure d, neurons 1 and 2 should synchronize if the respective contours are parts of one background face; neurons 3 and 4, which represent contours of the candlestick, should also synchronize. If there are two opposing faces, the temporal activity switches to synchrony between neurons 1 and 3, and 2 and 4, respectively (Figure 1.3e). How do neurons generates the synchronous spikes? A synfire chain is one of the network models that can generate synchronous spikes stably.

These properties of the synfire chain make it attractive, and there has been much research on the synfire chain. However, most of the research has been on the homogeneous type (Diesmann *et al.*, 1999; Câteau and Fukai, 2001); the inhomogeneous type has not been researched so thoroughly. Hamaguchi *et al.*researched the network with Mexican-Hat connectivity and showed that the network has several propagation mode, in which the speeds of propagation are different (Hamaguchi *et al.*, 2005a; 2005b; 2007). Figure 1.4 shows the relationship among the important works and this dissertation. A fatal defect of the homogeneous type is that the signals can be transmitted in only one pattern. This is not an efficient way to process information. We have modified the feedforward network so that signals can be transmitted in multiple modes.

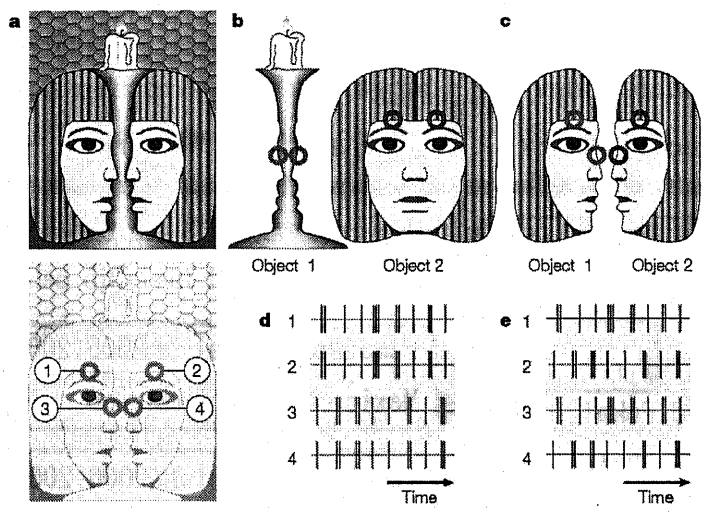

Figure 1.3: Figure adapted from Engel *et al.*, 2001, showing example of temporal binding model: a) bistable images (upper figure) and receptive fields of four neurons (lower figure), b) one-face interpretation, c) two-face interpretation, d) raster plot of spikes when neurons perceive situation b, and e) raster plot when neurons perceive situation c.

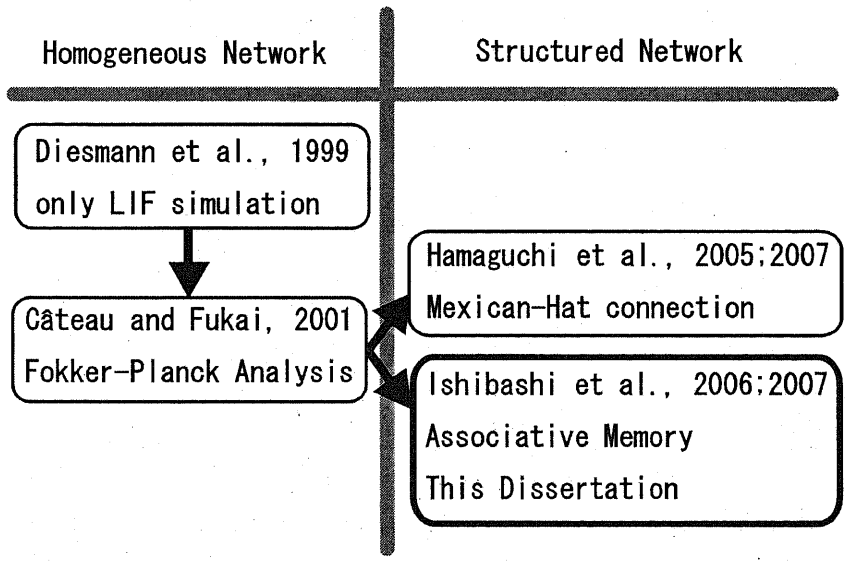

Figure 1.4: Schematic diagram of relationship among important works on synfire chains and this dissertation

1.3 Overview

To enable signal transmission of multiple patterns, we use associative memory. We constructed an associative network of the leaky integrate-and-fire (LIF) neuron model, as was done by Diesmann *et al.*, 1999. The LIF neuron model is a spiking neuron model. Spiking neuron models imitate the dynamics of the membrane potential of neurons, so they are more biologically plausible than simpler models like the rate neuron model and the binary neuron model.

Previous research on embedding multiple synfire chains in networks constructed of binary neurons (Bienenstock, 1995; Herrmann *et al.*, 1995) and integrate-and-fire neurons (Herrmann *et al.*, 1995; Aviel *et al.*, 2005) used random embedding. The neurons in the networks belong to a layer of a chain and can also different layers of another chain. As a result, the networks do not have ordered structure – they are quite similar to a randomly connected recurrent network. However, the highly ordered structures are often observed in the neural networks of animals, e.g., the six-layer structure of the mammalian neocortex and the DG-CA3-CA1 structure of the hippocampus (Kandel *et al.*, 2000). The activity of a structured network in which multiple synfire chains are embedded has not been reported. In this dissertation, I focus on the feedforward network. Because each synfire chain consists of feedforward connections, the structure seems natural. A feedforward network is also a good model for analyzing fast signal propagation (Panzeri *et al.*, 2001). As described in the next chapter, we can analyze the activity in such a feedforward network by using the Fokker-Planck method.

To enable transmission of multiple patterns, we embed multiple memory patterns by using the Hebbian learning rule (Hebb, 1949; Willshaw *et al.*1969; Hopfield, 1982; 1985; Domany and Meir, 1986; Meir and Domany, 1987a; 1987b; 1988; Amit 1989). The details of the associative feedforward network and the Fokker-Planck method are described in Chapter 2.

In Chapter 3, I describe in detail the properties of the associative feed-

forward network. An important feature is that the network can transmit embedded pattern packets stably as expected. The firing mode depends on input; some inputs result in spontaneous firing mode, some inputs result in synchronous propagation mode, and other inputs result in split propagation mode, which is not observed in the homogeneous network.

An important parameter of an associative network is the ratio of the number of neurons firing in a pattern to the total number of neurons. This ratio is conventionally called the "firing rate". To avoid possible confusion with the number of spikes, I call this ratio "pattern rate" (F). In Chapter 3, the pattern rate is set to 0.5, the simplest case. The properties of a network, especially storage capacity, strongly depends on the pattern rate. A network with a low pattern rate, a sparse network, has larger storage capacity and has been well researched (Willshaw *et al.*1969; Palm 1980; Golomb and Sompolinsky, 1990; Meunier *et al.*, 1988; Amari, 1989; Okada, 1996).

In Chapter 4, I describe the activity when the pattern rate does not equal 0.5. Although the property of synchronous propagation mode remains the same as that for a rate of 0.5, the property of split propagation mode changes qualitatively. When $F > 0.5$, the length of the split increases during propagation. When $F < 0.5$, the length decreases and eventually disappears, which is synchronous propagation mode. The activity in an associative network with $F \neq 0.5$ is described in Chapter 4. The most important difference between our associative feedforward network and a homogeneous feedforward network is its ability to transmit multiple patterns of pulse packets. Thus, an important question is how many kinds of pulse packets can the network transmit stably. "Storage capacity" denotes the number of patterns the network can transmit stably. Because of its importance, many researchers have investigated the storage capacity in the recurrent networks (Willshaw *et al.*, 1969; Palm, 1980; Hopfield, 1982; Amit *et al.*, 1985b) and randomly embedded synfire chains (Bienenstock, 1995; Aviel *et al.*, 2005). In Chapter 4, I also discuss the storage capacity of the associative feedforward network.

In Chapter 5, I describe the activity of the network when the embedded memory patterns are correlated. When they are, even activation of one memory pattern causes a split of spike timings between sublattices. I describe this mechanism and how sparse connection promotes synchronization even in this situation.

In Chapter 6, I summarize our research and discuss the future work.

Chapter 2

Network model

2.1 Associative feedforward network

In this dissertation, I describe an associative feedforward memory network with the Hebbian connections and constructed using the conventional method (Hebb 1949; Hopfield, 1982; Domany and Meir, 1986; Meir and Domany, 1987a; 1987b; 1988). Here I consider the feedforward network. Each layer consists of the same number of neurons, N. The index of a layer is l, and the index of a neuron in a layer is $i, j = 1, \ldots, N$. Memory patterns are embedded in the synaptic weights. We use $\xi_i^{l,\mu}$ to represents the μth memory pattern of the ith neuron in layer l. It takes a value of either $+1$ or 0. The number of memory pattern is p, and the index is $\mu = 1, \ldots, p$. Memory pattern $\xi_i^{l,\mu}$ is selected randomly in accordance with the probability

$$\text{Prob.}[\xi_i^{l,\mu} = +1] = F. \tag{2.1}$$

We call the probability of $\xi_i^{l,\mu} = +1$ the "pattern rate", i.e., F; and because of the randomness, there is no correlations between memory patterns. Memory pattern $\xi_i^{l,\mu} = +1$ means that the ith neuron in layer l would fire in memory pattern μ, and $\xi_i^{l,\mu} = 0$ means the neuron would be silent. We can regard these memory patterns in feedforward layers as the sequences of patterns. Here I assume that the sequences are activated deterministically.

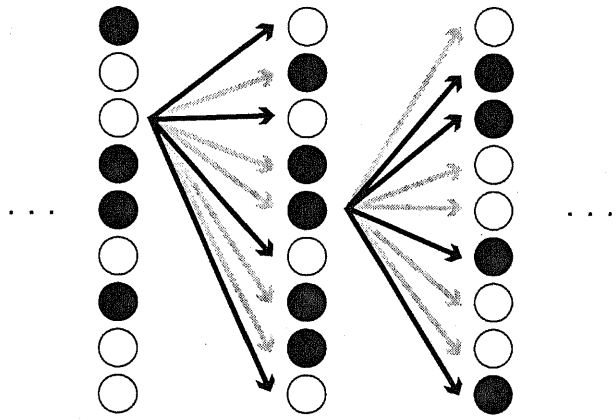

Figure 2.1: Schematic diagram of our associative feedforward network. Each circle means a neuron. The color shows one memory pattern. Black means $\xi_i^{l,\mu} = +1$, and white 0. Arrows show synaptic connections. Black arrows means excitatory connections, and gray ones inhibitory.

The activation of sequence branching and binding remains for future study.

Synaptic connection J_{ij}^l from the ith neuron in layer l to the jth neuron in layer $l+1$ is given by

$$J_{ij}^l = \frac{1}{F(1-F)N} \sum_{\mu=1}^{p} (\xi_j^{l+1,\mu} - F)(\xi_i^{l,\mu} - F). \tag{2.2}$$

This Hebbian learning rule is called the "covariance learning rule". The simplest concept of the Hebbian learning does not include the attenuation or inhibitory effect. Various types of expansions have been proposed for preventing the divergence and maintaining the balance between excitation and inhibition (Dayan and Sejnowski, 1993; Gerstner and Kistler, 2002). We adopted the covariance learning rule because it keeps the sum of synaptic weights equal to zero ($\sum_i J_{ij} = 0$) and because its existence is implied by the results of physiological experiments (Stanton and Sejnowski, 1989). The synaptic current is normalized by using $1/F(1-F)N$.

Figure 2.1 is a schematic diagram of this network.

We use the leaky integrate-and-fire (LIF) neuron model with white Gaus-

sian Noise as well as Diesmann *et al.* (Diesmann *et al.*, 1999). The dynamics of the membrane potential $v_i^l(t)$ is described as a stochastic differential equation,

$$\frac{\mathrm{d}v_i^l(t)}{\mathrm{d}t} = -\frac{v_i^l(t) - V_{\mathrm{rest}}}{\tau} + \frac{I_i^{l,\alpha}(t) + I_0}{C} + \eta(t), \tag{2.3}$$

where τ is the membrane time constant, V_{rest} is the resting potential, I_0 is the mean of the noisy input, $\eta(t)$ is the white Gaussian noise satisfying $< \eta(t) >= 0$ and $< \eta(t)\eta(t') >= 2D\delta(t-t')$. D means the diffusion coefficient. Input current $I_i^{l,\alpha}(t)$ is obtained by convoluting the presynaptic firing $I_i^l(t)$ with the α function $\alpha(t) = \alpha^2 t \exp(-\alpha t)$ as follows. β is a conversion constant.

$$I_i^{l,\alpha}(t) = \beta \int_0^\infty dt'\, \alpha(t') I_i^l(t-t'). \tag{2.4}$$

Input current $I_i^l(t)$ is derived from the sum of synaptic weights in which neurons fire. To equalize excitatory synaptic inputs for different pattern rate F, we set $I_i^l(t)$ proportional to $1/(1-F)$.

$$I_i^l(t) = \frac{1}{1-F} \sum_{j=1}^{N} J_{ji}^{l-1} \sum_{k=1}^{n} \delta(t - t_{j,k}^{l-1}), \tag{2.5}$$

where $t_{i,k}^l$ indicates the times that the ith neuron in layer l fires. The ith neuron in layer l has spiked n times until time t.

Membrane potential dynamics follow the spike-and-reset rule: when the membrane potential $v_i^l(t)$ reaches the threshold V_{th}, a spike is fired, and after the absolute refractoriness t_{ref}, the membrane potential is reset to the resetting potential V_{reset}. By implementing the absolute refractoriness, burst firings are inhibited and we can focus on pulse packets propagation.

For the following analysis, we introduce the order parameter function $m^{l,\mu}(t)$, namely the overlap, defined by

$$m^{l,\mu}(t) = \frac{1}{F(1-F)N} \sum_{i=1}^{N} (\xi_i^{l,\mu} - F) \sum_{k=1}^{n} \delta(t - t_{i,k}^l). \tag{2.6}$$

Here, the overlap means how much the firing pattern matches the μth memory pattern in layer l. If neurons with their memory patterns $\xi_i^{l,\mu} = +1$ fire once, then $\int_{-\infty}^{\infty} dt\, m^{l,\mu}(t) = 1$. By using the overlap, $I_i^l(t)$ can be rewritten as

$$I_i^l(t) = \sum_{\mu=1}^{p} \frac{\xi_i^{l,\mu} - F}{1-F} m^{l-1,\mu}(t). \tag{2.7}$$

This means that the synaptic current to a neuron depends only on the overlap of the preceding layer and its memory patterns. Here we can see that $I_i^l(t)$ need to be proportional to $1/(1-F)$ so that the excitatory inputs does not change with different pattern rate F.

Throughout this dissertation, the parameter values are fixed as follows: $V_{\text{rest}} = V_{\text{reset}} = 0$ mV, $V_{\text{th}} = 15$ mV, $t_{\text{ref}} = 1$ ms, $\tau = 10$ ms, $I_0 = 0.075$ pA, $C = 100$ pF, $D = 0.5$, $\alpha = 2$ ms^{-1}, and $\beta = 0.17$ pA. The number of neurons per layer is set to $N = 5000$ in whole the LIF simulations.

2.2 Fokker-Planck method

In this section, we introduce the analytical method of calculating the membrane potential distribution. First, we define a vector whose elements are memory patterns of the ith neuron as $\boldsymbol{\xi}_i^l = (\xi_i^{l,1}, \xi_i^{l,2}, \ldots, \xi_i^{l,p})$. Each element takes on a value $+1$ or 0, and thus this vector has 2^p combinations. We can define 2^p groups according to $\boldsymbol{\xi}_i^l$ values. We call each group a sublattice and we discriminate each sublattice with the vector $\boldsymbol{\xi} = (\xi^1, \xi^2, \ldots, \xi^p)$. Each element ξ^μ takes on $+1$ or 0 values. Here we define $d(\boldsymbol{\xi})$ as the ratio of the number of neurons belonging to the sublattice $\boldsymbol{\xi}$ to the whole number of neurons and $d(\boldsymbol{\xi})$ is described as follows:

$$d(\boldsymbol{\xi}) = \prod_{\mu=1}^{p} \left(\xi^\mu F + (1-\xi^\mu)(1-F)\right). \tag{2.8}$$

Neurons belonging to the same sublattice receive the same synaptic current, because the synaptic current depends on only the overlaps and its memory pattern $\boldsymbol{\xi}_i^l$ (see equation (2.7)). The distribution of the membrane potential is known to evolve according to the Fokker-Planck equation (Risken, 1996),

$$\frac{\partial}{\partial t}P_{\boldsymbol{\xi}}^l(v,t) = -\frac{\partial}{\partial v}j_{\boldsymbol{\xi}}^l(v,t) + \delta(v - V_{\text{reset}})d(\boldsymbol{\xi})\nu_{\boldsymbol{\xi}}^l(t - t_{\text{ref}}), \tag{2.9}$$

$$j_{\boldsymbol{\xi}}^l(v,t) = -\left(\frac{v - V_{\text{rest}}}{\tau} - \frac{I_{\boldsymbol{\xi}}^{l,\alpha}(t) + I_0}{C} + \frac{\partial}{\partial v}D\right)P_{\boldsymbol{\xi}}^l(v,t). \tag{2.10}$$

$P_{\boldsymbol{\xi}}^l(v,t)$ is the distribution of the membrane potentials of the neurons belonging to sublattice $\boldsymbol{\xi}$, and $\nu_{\boldsymbol{\xi}}^l(t) = j_{\boldsymbol{\xi}}^l(V_{\text{th}},t)/d(\boldsymbol{\xi})$ is the flow of probability across the threshold V_{th} per second per neuron, that is to say firing rate; the number of spikes per second per neuron. $P_{\boldsymbol{\xi}}^l(v,t)$ and $\nu_{\boldsymbol{\xi}}^l(t)$ satisfy the normalization condition:

$$\int_{-\infty}^{V_{th}} dv\, P_{\boldsymbol{\xi}}^l(v,t) + d(\boldsymbol{\xi})\int_0^{t_{\text{ref}}} d\tau\, \nu_{\boldsymbol{\xi}}^l(t-\tau) = d(\boldsymbol{\xi}). \tag{2.11}$$

Here we define the overlap vector, $\boldsymbol{m}^l(t) = (m^{l,1}(t), m^{l,2}(t), \ldots, m^{l,p}(t))$. From equations (2.4) and (2.7), we can describe the synaptic current $I_{\boldsymbol{\xi}}^{l,\alpha}(t)$ by using $\boldsymbol{\xi}$ and $\boldsymbol{m}^l(t)$ as follows:

$$I_{\boldsymbol{\xi}}^{l,\alpha}(t) = \beta\int_0^{\infty} dt'\, \alpha(t) I_{\boldsymbol{\xi}}^l(t-t'), \tag{2.12}$$

$$I_{\boldsymbol{\xi}}^l(t) = \frac{\boldsymbol{\xi} - F\boldsymbol{I}}{1-F}\cdot \boldsymbol{m}^{l-1}(t), \tag{2.13}$$

where $\boldsymbol{I}$ is the vector whose all elements are 1 and size is p.

From equation (2.6), we can describe the overlap $m^{l,\mu}(t)$ by using firing rate $\nu_{\boldsymbol{\xi}}^l(t)$ as

$$m^{l,\mu}(t) = \frac{1}{F(1-F)}\sum_{\boldsymbol{\xi}} d(\boldsymbol{\xi})\nu_{\boldsymbol{\xi}}^l(\xi^\mu(1-F) - (1-\xi^\mu)F). \tag{2.14}$$

Here we can describe the network dynamics only by using macroscopic parameters $P^l_{\boldsymbol{\xi}}(v,t)$, $\nu^l_{\boldsymbol{\xi}}(t)$, and $\boldsymbol{m}^l(t)$.

In this dissertation, we numerically calculate the Fokker-Planck equation with the Chang-Cooper Method (Chang and Cooper, 1970; Park and Petrosian, 1996). At the boundary, we stock the flow at $V_{\rm th}$ and after $t_{\rm ref}$ add the stocked flow to the probability at $V_{\rm reset}$ (see equation (2.9)).

The description with the Fokker-Planck method is consistent with the LIF simulation in the limit of the number of neurons belonging to each sublattice $Nd(\boldsymbol{\xi}) \to \infty$. Because the minimum value of $d(\boldsymbol{\xi})$ is less than 2^{-p}, we restrict the total number of memory patterns to $p \sim O(1)$.

Chapter 3

Basic associative feedforward network

3.1 Introduction

The purpose of this dissertation is to clarify the ability of a simple neural network to transmit signals. Diesmann *et al.* showed that a homogeneous feedforward network transmits a pulse packet stably and there is only one propagation pattern. In this dissertation I describe properties of an associative feedforward network. I address whether it can transmit pulse packets that correspond to the embedded memory patterns. In this chapter, I present the analysis for pattern rate $F = 0.5$, meaning that the half the neurons in the network would fire in a pulse packet.

In the following sections I describe our analysis using LIF simulation and the Fokker-Planck method. In this chapter, I consider the case in which the number of memory patterns, p, is much smaller than the number of neurons in a layer, N. Thus, the results from LIF simulation are always consistent with those from the Fokker-Planck method. In Section 3.2, I discuss the simplest case, i.e., when single memory pattern is activated. Next, I discuss the case in which two memory patterns are activated in Section 3.3. In Subsection 3.3.1, I discuss the simultaneous activation of two memory patterns and, in

Subsection 3.3.2, the successive activation of two memory patterns. Section 3.4 summarizes the chapter.

3.2 Activation of single memory pattern

In this section, I address whether the associative feedforward network can transmit synchronous spikes of embedded memory patterns stably by using the LIF simulation and the Fokker-Planck method. Throughout this dissertation, I activate the network by input current into the first layer of the network and the initial condition is a stationary distribution for no external input ($I_i^l(t) = 0$). We use the overlap as an index of how firing patterns match the memory pattern. For the first layer activation, we consider the virtual layer and describe the overlap on the virtual layer of memory pattern 1 (the activated memory pattern) as a Gaussian function with standard deviation σ and total volume m. In this section, the volumes of the other memory patterns (the unactivated memory patterns) are set to 0;

$$m^{0,\mu}(t) = \begin{cases} \dfrac{m}{\sqrt{2\pi}\sigma} \exp\left(\dfrac{(t-t_0)^2}{2\sigma^2}\right) & \mu = 1, \\ 0 & \mu \neq 1. \end{cases} \tag{3.1}$$

First, we simulated the membrane potential dynamics of the LIF neurons. We calculate the input currents to neurons from equations (2.4) and (2.7), membrane potential dynamics from equation (2.3), and the overlaps of the first memory pattern $m^{l,1}(t)$ from equation (2.6). I plotted the overlaps as dashed lines in Figures 3.1(a) and 3.1(b). Each figure shows the overlaps of the five layers vertically. Figure 3.1(a) is the case that the total volume of the overlap of the virtual layer is set to $m = 0.6$, and Figure 3.1(b) is the case with $m = 0.4$. In Figure 3.1(a), the temporal profile of the overlap becomes sharper as the activity propagates through the layers. Therefore, the activated memory pattern synchronously propagates as a pulse packet under this condition. We call this mode "embedded pattern propagation mode". In

contrast, in Figure 3.1(b), the overlap disappears as the activity propagates. This means that the activated memory pattern does not propagate under the latter condition. This is the same mode as the spontaneous firing mode.

Next, we analyze the dynamics of the network by the Fokker-Planck method. When the input overlap of a memory pattern is 0, the synaptic current does not depend on the memory pattern (Eq. (2.7)). Therefore we does not need to consider the sublattice of the unactivated memory patterns. In this situation, it is enough to pay attention to only the sublattice of the activated memory pattern. We calculate 2 membrane potential distributions, $P^l_+(v,t)$ and $P^l_-(v,t)$, and 2 firing rates, $\nu^l_+(t)$ and $\nu^l_-(t)$ on each layer. The subscript index $(+)$ means $\boldsymbol{\xi} = (+1)$ sublattice and $(-)$ means $\boldsymbol{\xi} = (0)$. We calculate the input current to the neurons belonging to each sublattice from equations (2.12) and (2.13), membrane potential distributions and firing rates from the Fokker-Planck equation (see equation (2.9)), and the overlaps of the first memory pattern $m^{l,1}(t)$ from equation (2.14). I plotted the overlaps as solid lines in Figures 3.1(a) and 3.1(b). Figures 3.1(a) and 3.1(b) show the consistency between the results of the LIF simulation and those of the Fokker-Planck method.

We choose the overlap of the virtual layer to be the Gaussian function with total volume m and standard deviation σ. Now, we evaluate the total volume m' and the standard deviation σ' of the overlap of the first layer by approximating the overlap with the Gaussian function by using the method of least squares. Though the overlap of the first layer is precisely not the Gaussian Function but a little temporally tailed function, the difference is small and the approximation works well. Figure 3.2 shows the normalized vector from (m,σ) to (m',σ') as well as the Diesmann *et al.*, 1999 and Câteau and Fukai, 2001. Figure 3.2(a) shows the results of the LIF simulations and Figure 3.2(b) shows those of the Fokker-Planck method. Figure 3.2 shows that if the initial activation is strong and synchronous enough, the overlap converges the attractor on the left. This attractor means that the spike

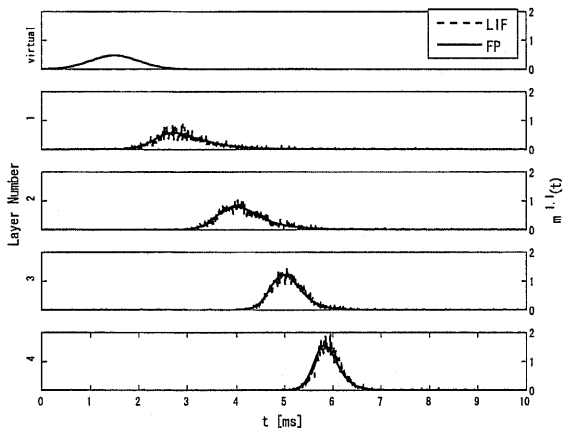

(a) $m = 0.6$

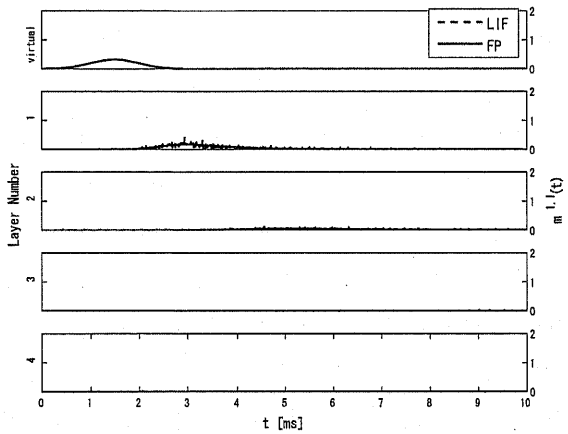

(b) $m = 0.4$

Figure 3.1: Overlaps $m^{l,1}(t)$ $(l = 0 \cdots 4)$ when the total volume of the overlap on the virtual layer is set to $m = 0.6$(a) or $m = 0.4$(b), and the standard deviation is set to $\sigma = 0.5$ ms. The dashed line is obtained with the LIF simulation, and the solid line with the Fokker-Planck method. We define t_0, when $m^{0,1}(t)$ takes a peak value, as $3\sigma = 1.5$ ms.

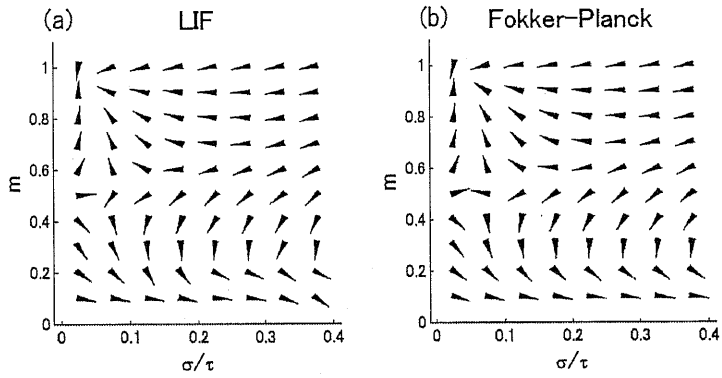

Figure 3.2: Each arrow means the change from an input overlap to an output overlap. The input overlaps are Gaussian functions, and the output overlaps are approximated as Gaussian functions. (a) LIF simulation result, (b) Fokker-Planck method result.

pattern almost matches the activated memory pattern and the spikes are highly synchronized. It indicates that this network works as a synfire chain and the activated memory pattern propagates as a pulse packet. In contrast, when the initial input is too weak or too dispersed, the overlap disappears in the lower right region. Those results of the LIF simulation (Figure 3.2(a)) are highly consistent with those of the Fokker-Planck method (Figure 3.2(b)).

Next, we analyze the change of the overlap when we change the diffusion coefficient D. Figure 3.3 shows the result. Figure 3.3 is the case of (a) $D = 0.25\text{mV}^{\,2}\cdot\text{ms}^{-1}$, (b)$D = 0.5\text{mV}^{\,2}\cdot\text{ms}^{-1}$ (the standard situation), (c)$D = 1.0\text{mV}^{\,2}\cdot\text{ms}^{-1}$, and (d)$D = 2.5\text{mV}^{\,2}\cdot\text{ms}^{-1}$. Figure 3.3 (a-c) shows that the smaller diffusion coefficient D is, the shaper the temporal profile of overlap is and the larger value of overlap is, and however the change is small and the basin of attraction also shows little change. On the other hand, 3.3(d) shows that if the diffusion amplitude is too large, neurons tend to burst and the stable propagation collapse. These results imply that the diffusion coefficient does not effect the dynamics of synchronous signal propagation so much unless it reaches the threshold.

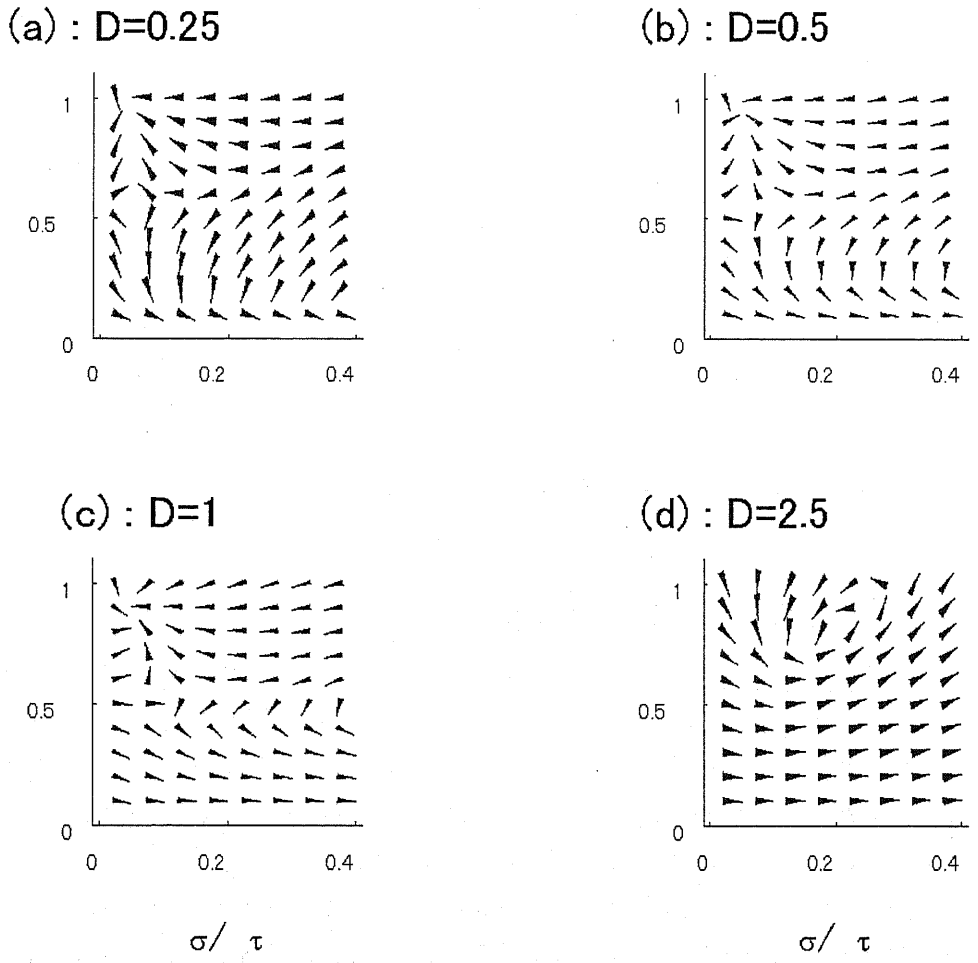

Figure 3.3: Each arrow means the change from an input overlap to an output overlap. The input overlaps are Gaussian functions, and the output overlaps are approximated as Gaussian functions. 4 figures have different diffusion coefficient; (a) $D = 0.25\text{mV}^{\,2}\cdot\text{ms}^{-1}$, (b)$D = 0.5\text{mV}^{\,2}\cdot\text{ms}^{-1}$(the standard situation), (c)$D = 1.0\text{mV}^{\,2}\cdot\text{ms}^{-1}$, and (d)$D = 2.5\text{mV}^{\,2}\cdot\text{ms}^{-1}$

Finally, I analyze the change of the overlap when we change the time constant of α function. Figure 3.4 shows the result. Figure 3.3 is the case of (a)$\alpha = 8.0\text{ms}^{-1}$, (b)$\alpha = 4.0\text{ms}^{-1}$, (c)$\alpha = 2.0\text{ms}^{-1}$ (the standard situation), and (d)$\alpha = 1\text{ms}^{-1}$. Figure 3.4 (a-d) shows that the standard deviation of the temporal profiles of the overlap at the attractor shows strong dependence on α.

Hereafter in this chapter, we show only the results of the Fokker-Planck method, as all of the results are consistent with the LIF simulations.

3.3 Activation of two memory patterns

In the previous section, I showed that in an associative feedforward network an activated memory pattern could propagate as a pulse packet. Here we focus on the temporal profiles of the network activities when multiple memory patterns are activated. In this section we analyze the simplest case: the activation of two memory patterns with an arbitrary interval T_{delay}. Figure 3.5 is a schematic diagram of the temporal profiles of the overlaps of the activated memory patterns. Here we consider two situations: simultaneous activation ($T_{\text{delay}} = 0$) and successive activation ($T_{\text{delay}} > 0$). In both situations, we divide neurons into sublattices according to the two memory patterns, because the overlaps of unactivated memory patterns are always 0 and the unactivated memory patterns do not effect the activities of the neurons. I describe the focused sublattices $\boldsymbol{\xi} = (+1,+1), (+1,0), (0,+1)$, and $(0,0)$ as $(++), (+-), (-+)$, and $(--)$. The membrane potential distributions are accordingly divided into the following groups: $P^l_{++}, P^l_{+-}, P^l_{-+}$, and P^l_{--}. We denote the firing rates of each sublattice as $\nu^l_{++}, \nu^l_{+-}, \nu^l_{-+}$, and ν^l_{--}.

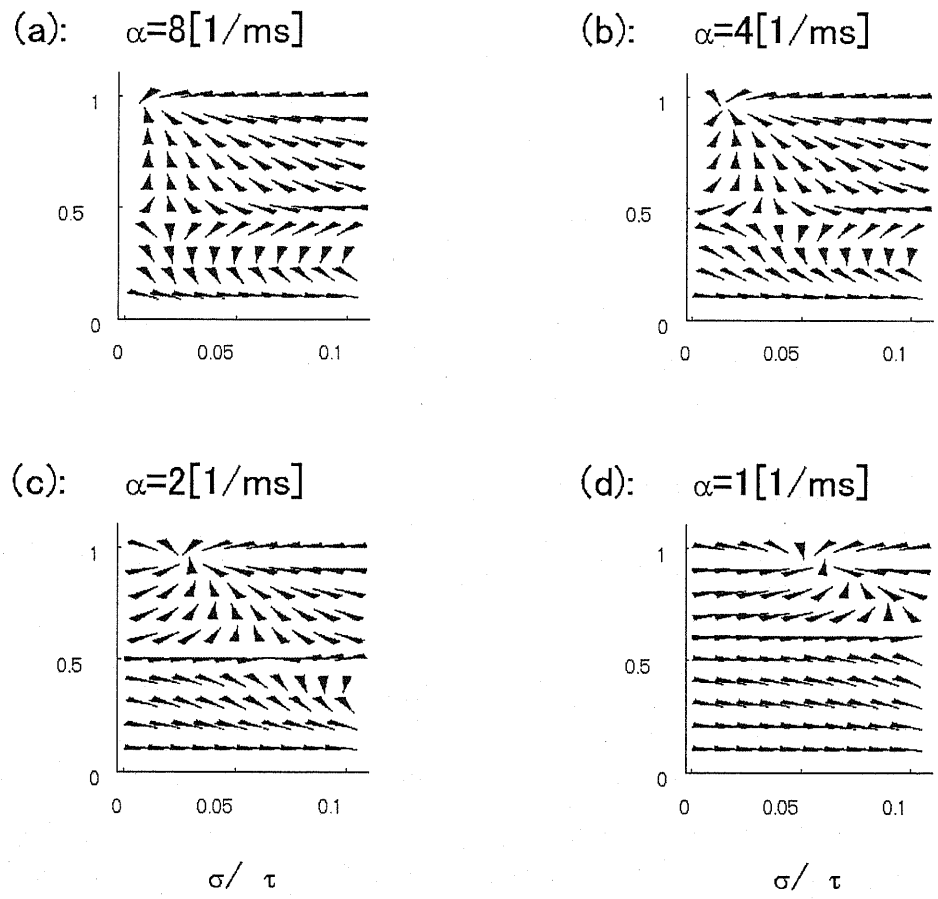

Figure 3.4: Each arrow means the change from an input overlap to an output overlap. The input overlaps are Gaussian functions, and the output overlaps are approximated as Gaussian functions. 4 figures have different diffusion coefficient; (a)$\alpha = 8.0\text{ms}^{-1}$, (b)$\alpha = 4.0\text{ms}^{-1}$, (c)$\alpha = 2.0\text{ms}^{-1}$, and (d)$\alpha = 1\text{ms}^{-1}$

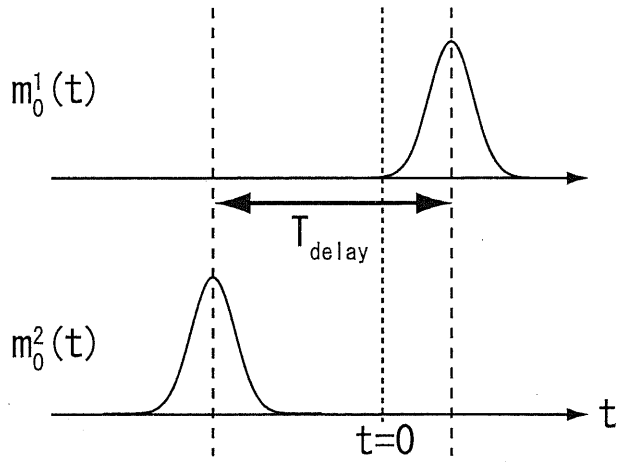

Figure 3.5: Schematic diagram of the activation of two memory patterns. We activate memory pattern 1 T_{delay} after memory pattern 2. We define the time of the onset of the first memory pattern activation as 0.

3.3.1 Simultaneous activation of two memory patterns

Let us consider the case in which two memory patterns are activated simultaneously. The overlaps of the virtual layer are described as follows:

$$m^{0,\mu}(t) = \begin{cases} \dfrac{m^\mu}{\sqrt{2\pi}\sigma^\mu} \exp\left(\dfrac{(t-t_0^\mu)^2}{2\sigma^{\mu 2}}\right) & \mu = 1, 2, \\ 0 & \mu \neq 1, 2. \end{cases} \tag{3.2}$$

Regarding simultaneous activation, we assume that neurons on the virtual layer do not fire no more than twice during our focus. The sum of total volumes of overlaps satisfies $m^1 + m^2 \leq 1$ because we consider two orthogonal memory patterns. Here, we set that $m^1 + m^2 = 1, \sigma^1 = \sigma^2 = 0.5$ ms, and $t_0^1 = t_0^2$. We change only the ratio of m^1 to m^2.

First, I explain the simplest situation; $m^1 = 1$ and $m^2 = 0$. As we have seen before, the overlap of the second memory pattern was always 0, and memory pattern 1 propagated as a pulse packet as in Figure 3.1(a).

Second, we analyzed balanced activation; $m^1 = m^2 = 0.5$. Figure 3.6 shows the temporal profiles of the overlaps. Throughout the observation,

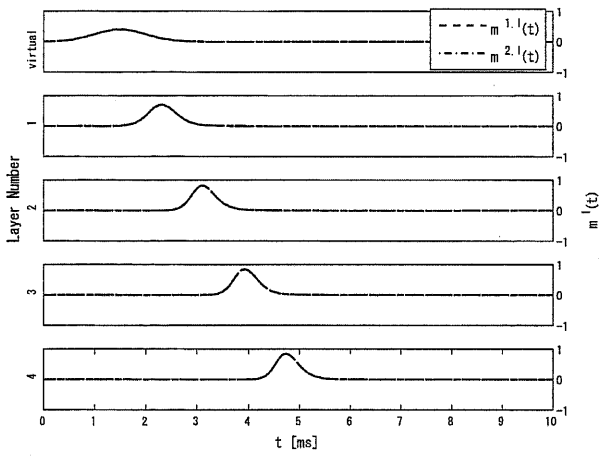

Figure 3.6: Overlaps $m^{l,\mu}(t)$ when two memory patterns are activated with the same strength; $m_1 = m_2 = 0.5$. We define t_0^1, when $m^{0,1}(t)$ takes a peak value, as $3\sigma^1 = 1.5$ ms.

both overlaps $m^{l,1}(t), m^{l,2}(t)$ have the same value and their total volumes were $\int_{-\infty}^{\infty} dt\, m^{\mu,l}(t) \sim 0.5$. This situation seems to indicate that both memory patterns propagate with their intermediate levels. We call this mode "mixed pattern propagation mode".

In order to elucidate which sublattices contain firing neurons, we focus on the firing rate of each sublattice. Figure 3.7 shows the firing rates $\nu_{\boldsymbol{\xi}}^l$. This figure shows that in the mixed pattern propagation mode spikes of $\boldsymbol{\xi} = (++)$ propagate stably. Although the $\boldsymbol{\xi} = (++)$ sublattice is not a memory pattern, the activity of $\boldsymbol{\xi} = (++)$ propagates as a pulse packet. Therefore, the associative feedforward network is a synfire chain in which not only memory patterns but also their mixed pattern propagates as pulse packets.

Next, we gradually increase m^1 from 0.5 to 1 while stipulating that $m^1 + m^2 = 1$. As long as m^1 is approximately smaller than 0.7, $m^{1,l}(t) > m^{2,l}(t)$ early in several layers. However the network finally converges to the mixed pattern propagation mode, as in Figures 3.6 and 3.7. In contrast, when m^1 is larger than a certain threshold, $m^{1,l}(t)$ has two peaks, and $m^{2,l}(t)$

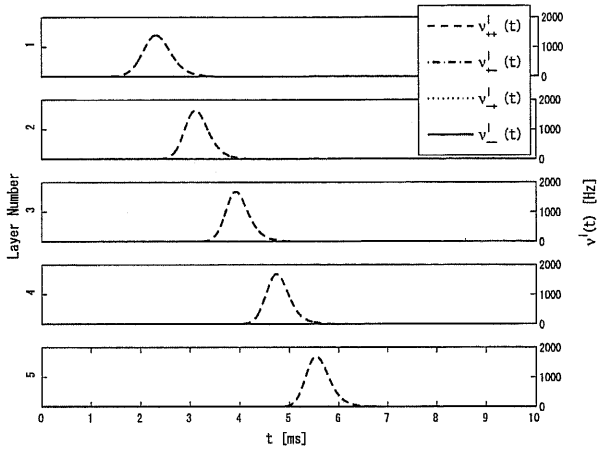

Figure 3.7: Firing rate $\nu_{\boldsymbol{\xi}}^{l}(t)$ of each sublattice when two memory patterns are simultaneously activated with the same strength($m_1 = m_2 = 0.5$).

has one positive peak and one negative peak. Figure 3.8 plots the overlaps for $m^1 = 0.8$ and $m^2 = 0.2$. After convergence, $\int_{-\infty}^{\infty} dt\, m^{1,l}(t) \sim 1$ and $\int_{-\infty}^{\infty} dt\, m^{2,l}(t) \sim 0$. In this regard, this situation is similar to when only the one memory pattern is activated. However it is different in that the overlaps have two peaks.

Similar to Figure 3.7, Figure 3.9 shows the firing rate of each sublattice for this case. Figure 3.9 indicates that neurons in $\boldsymbol{\xi} = (++)$ and $(+-)$ sublattices fire synchronously in each sublattice but at different timings between the sublattices. We call this mode "split propagation mode" because of the split of spike timings. This difference is due to the difference in synaptic current strengths. In the first layer, $I_{++}(t) = \frac{1}{2}(m^{1,l}(t) + m^{2,l}(t)) > I_{+-}(t) = \frac{1}{2}(m^{1,l}(t) - m^{2,l}(t))$ because $m^{2,l}(t) > 0$. Therefore, neurons in the $(++)$ sublattice receiving the larger current fire earlier than those in the $(+-)$ sublattice.

The split of spike timings does not grow after convergence in the split

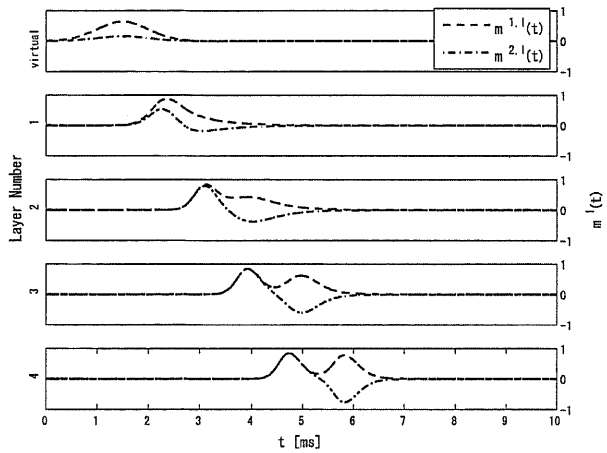

Figure 3.8: Overlaps $m^{l,\mu}(t)$ when memory pattern 1 is more strongly activated than memory pattern 2 ($m_1 = 0.8$, $m_2 = 0.2$).

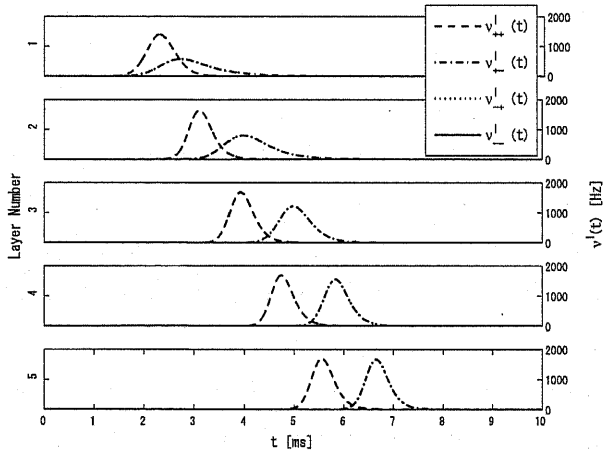

Figure 3.9: Firing rate $\nu^l_{\boldsymbol{\xi}}(t)$ of each sublattice when memory pattern 1 is more strongly activated than memory pattern 2; $m_1 = 0.8$, $m_2 = 0.2$.

propagation mode. To elucidate the reason, we rewrite $I_{\boldsymbol{\xi}}^{l+1}$ as follows:

$$\begin{aligned} I_{++}^{l+1} &= \frac{1}{2}\left(m^{1,l}(t) + m^{2,l}(t)\right) \\ &= \frac{1}{4}\Big(\nu_{++}^{l}(t) + \nu_{+-}^{l}(t) - \nu_{-+}^{l}(t) - \nu_{--}^{l}(t) \\ &\qquad + \nu_{++}^{l}(t) + \nu_{-+}^{l}(t) - \nu_{+-}^{l}(t) - \nu_{--}^{l}(t)\Big) \\ &= \frac{1}{2}\left(\nu_{++}^{l}(t) - \nu_{--}^{l}(t)\right), \end{aligned} \tag{3.3}$$

Similarly,

$$I_{+-}^{l+1} = \frac{1}{2}\left(\nu_{+-}^{l}(t) - \nu_{-+}^{l}(t)\right), \tag{3.4}$$

$$I_{-+}^{l+1} = \frac{1}{2}\left(\nu_{-+}^{l}(t) - \nu_{+-}^{l}(t)\right) = -I_{+-}^{l+1}, \tag{3.5}$$

$$I_{--}^{l+1} = \frac{1}{2}\left(\nu_{--}^{l}(t) - \nu_{++}^{l}(t)\right) = -I_{++}^{l+1}. \tag{3.6}$$

From these equations, the activities of the $\boldsymbol{\xi} = (++), (--)$ sublattices independently propagate from $(+-), (-+)$ sublattices. Note that this independence cannot be achieved by the activation of more than 3 memory patterns. In the activation of two memory patterns, the activity of the $(++)$ sublattice independently propagates from that of $(+-)$. After each activity reaches a synchronous mode, which is the attractor in Figure 3.2, both activities propagate at the same speed.

This analysis of firing rate dynamics indicates that the boundary between the mixed state and the split propagation mode is the boundary of the propagation of $(+-)$ sublattice activity.

Finally, we gradually increased m^1 to 1. As m^1 became larger, the split of spike timings between the 2 sublattices became smaller and finally vanished when $m^1 = 1$. Thus, we can consider the single pattern propagation as a special case of split propagation mode.

In summary, simultaneous activation under the restriction of $m^1 + m^2 = 1$ gives rise to two modes, mixed pattern propagation mode and split propa-

gation mode. If $|m^1 - m^2|$ is small enough, the network converges to mixed pattern propagation mode; otherwise it converges to split propagation mode.

3.3.2 Successive activation of two memory patterns

Câteau and Fukai reported that when they activated two pulse packets successively with a short interval, the following pulse packet did not propagate because of hyperpolarization caused by the preceding pulse packet's propagation (Câteau and Fukai, 2001).

In this subsection I described the case in which two memory patterns are successively activated with a short interval, $T_{\text{delay}} > 0$. By contrast with the previous subsection, we do not restrict the number of spikes which is in contrast to the simultaneous activation. Thus $m^1 + m^2$ can take more than 1. For simplicity, we assume that the overlaps of the virtual layer of both memory patterns take on the same values except for the timing, and that the parameters of the Gaussian functions describing the virtual layer overlaps are $m^1 = m^2 = 0.7$, and $\sigma^1 = \sigma^2 = 0.5$ ms in equation (3.2). We activate memory pattern 1 (the following pattern) after memory pattern 2 (the preceding pattern) (Figure 3.5).

When T_{delay} is much larger than the membrane time constant $\tau(= 10$ ms), for example $T_{\text{delay}} = 50$ ms, the $\boldsymbol{\xi} = (++)$ and $(-+)$ sublattices are simultaneously activated by the preceding pattern activation, and the $\boldsymbol{\xi} = (++)$ and $(+-)$ sublattices are almost simultaneously activated by the following pattern activation (Figure 3.10). In this situation, the following memory pattern seemed to propagate normally without being affected by the preceding memory pattern's propagation.

However, when the interval T_{delay} is decreased, the spikes of neurons belonging to $\boldsymbol{\xi} = (+-)$ sublattice are gradually delayed compared with those of $(++)$ neurons during the following pattern propagation. Figure 3.11 shows the firing rate of each sublattice when the interval $T_{\text{delay}} = 20$ ms. This mode is same as the split propagation mode in the previous subsection.

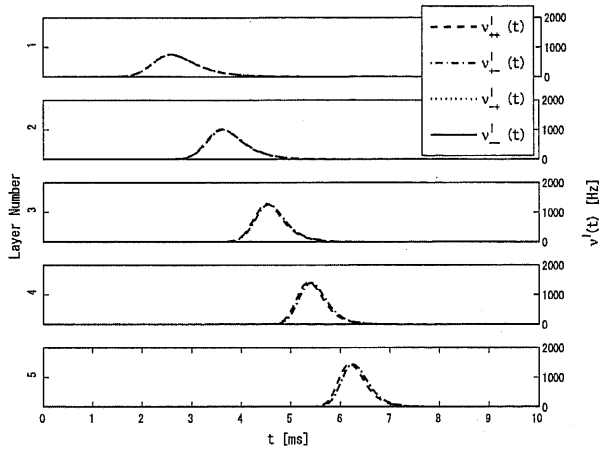

Figure 3.10: Firing rate of each sublattice when we activate the pattern 1 $T_{\text{delay}} = 50$ ms after the activation of memory pattern 2. t_0^1, when $m^{0,1}(t)$ has a peak value, is defined as $3\sigma^1 = 1.5$ ms.

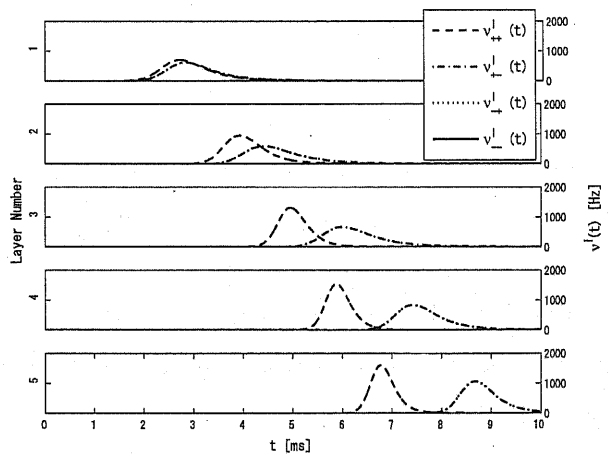

Figure 3.11: Firing rate of each sublattice when we activate the pattern 1 $T_{\text{delay}} = 20$ ms after the activation of memory pattern 2. t_0^1, when $m^{0,1}(t)$ has a peak value, is defined as $3\sigma^1 = 1.5$ ms.

To investigate the reason for this delay, we plot the membrane potential distribution of the first layer of each sublattice $P^l_{\boldsymbol{\xi}}$ after the propagation of the preceding pattern ($\mu = 2$ memory pattern) in Figure 3.12. During propagation of the preceding pattern, neurons in the $\boldsymbol{\xi} = (++)$ and $(-+)$ sublattices fire and their membrane potentials are reset to V_{reset} (Figure 3.12 dashed line). In contrast, neurons in the $(+-)$ and $(--)$ sublattices hyperpolarize because of the inhibitory current (Figure 3.12, solid line). Therefore when the input from the following pattern arrives, neurons in the $(+-)$ sublattice take more time than the ones in the $(++)$ sublattice to reach the threshold V_{th}. This is the origin of the delay. Membrane potentials relax with the membrane time constant τ. Therefore this effect remains for the order of the membrane time constant.

In the deeper layers, a once dispersed $(+-)$ pulse packet develops into a synchronized pulse packet, and the interval between the preceding pattern and $(+-)$ pulse packet approaches a certain value, which is long enough for the membrane potential distribution of the $(+-)$ sublattice to relax to the stationary state. These dynamics are independent of the $(++)$ sublattice dynamics. The $(++)$ pulse packet also develops into the synchronized state, and the interval between the preceding pattern and the $(++)$ pulse packet also converges to a certain interval. Therefore, the delay between $(++)$ and $(+-)$ also converges to a certain delay period.

If the time interval is further decreased, the activity of the $(+-)$ sublattice does not propagate after the following pattern activation. Figure 3.13 shows the firing rate of each sublattice when the time interval is $T_{\text{delay}} = 15$ms. This figure shows that only the activity of the $(++)$ sublattice propagates whereas that of $(+-)$ dies out. This is the mixed pattern propagation mode described in Figure 3.7. The activity of $(+-)$ does not propagate because the smaller T_{delay} is, the more the inhibitory effect remains and it is more difficult for neurons belonging to $(+-)$ to fire when the following pattern is activated.

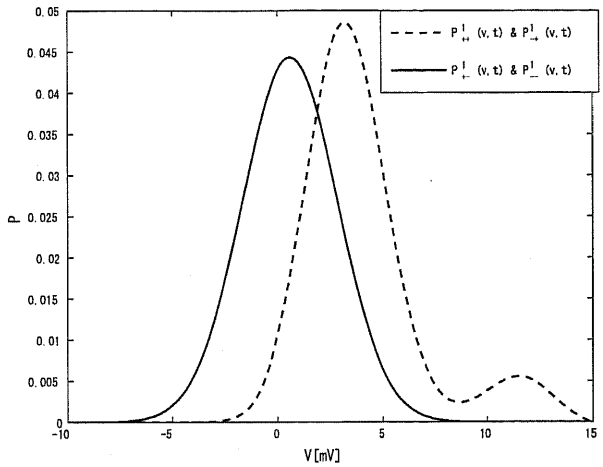

Figure 3.12: Membrane potential distribution of the first layer of each sublattice after propagation of the preceding pattern (memory pattern 2), 6.5 ms after t_0^2. The membrane potential distribution of the $\boldsymbol{\xi} = (++), (-+)$ sublattice is plotted as the dashed line and that of $(+-), (--)$ as the solid line.

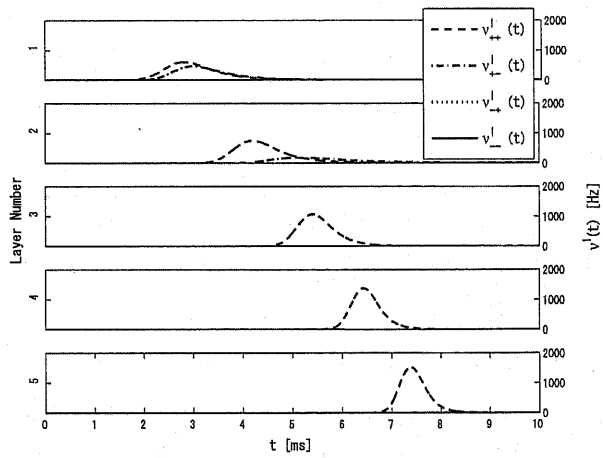

Figure 3.13: Firing rate of each sublattice when we activate memory pattern 1 $T_{\text{delay}} = 15$ ms after the activation of memory pattern 2.

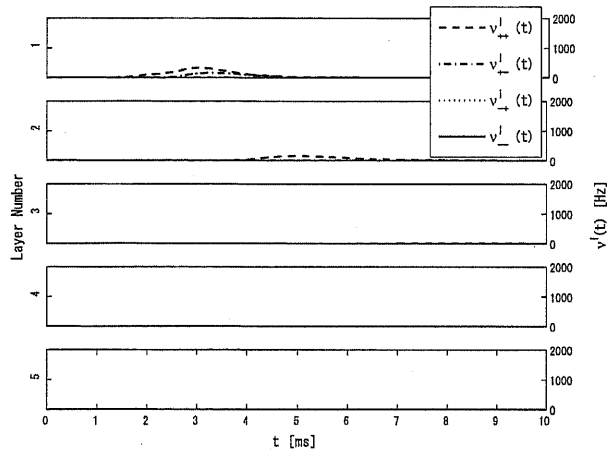

Figure 3.14: Firing rate of each sublattice when we activate the pattern 1 $T_{\text{delay}} = 8$ ms after the activation of memory pattern 2. t_0^1, when $m^{0,1}(t)$ has a peak value, is defined as $3\sigma^1 = 1.5$ ms.

When the time interval is decreased even further, for example $T_{\text{delay}} =$ 8ms, even the activity of the (++) sublattice does not propagate (Figure 3.14). This is because of hyperpolarization after spikes in the preceding activation. Therefore it is difficult even for neurons belonging to the (++) sublattice to fire when the first memory pattern is activated. This phenomenon is similar to the one reported by Câteau and Fukai, 2001.

3.4 Summary and discussion

In this dissertation, I described a model of an associative feedforward network constructed of LIF neurons and its analysis using the Fokker-Planck method.

First, I showed that the network has propagation modes of the embedded memory patterns. These modes are observed when one embedded memory pattern is activated strongly and synchronously.

Second, I showed that not only embedded patterns but also mixed patterns propagate synchronously when two memory patterns are activated simultaneously. The split propagation mode is observed when there is unbal-

anced activation of two memory patterns.

Finally, I showed that the successive activation of two memory patterns produces the mixed pattern propagation mode and the split propagation mode. The mode of the network activity and the propagation of sublattices depend on the interval between the two activations.

The difference between the conventional binary neuron network and our network is the stability around memory patterns. The conventional network converges to embedded pattern propagation mode or mixed pattern propagation mode, not to split propagation mode. The split propagation mode is characteristic of spiking neuron models because spiking neuron models driven by inputs of different strengths fire at different timings. In contrast, binary neurons fire simultaneously even if the strength are unequal as long as the current reaches the threshold. Simultaneous firing means the network is in memory pattern mode. The meaning of the split of spike timings is unknown. The split might transmit the information of unbalanced input. In the next chapter, I discuss the stability of the split propagation mode when the pattern rate is not 0.5.

Chapter 4

Sparsely and densely connected associative feedforward network

4.1 Introduction

In the previous chapter, I discussed the signal propagation when the pattern rate of the network is 0.5, which means that half the neurons in a layer would fire in the embedded pattern propagation mode. How does the activity of the network differ when the pattern rate is not 0.5?

In this chapter, I discuss how signal propagation depends on the pattern rate for sparsely and densely connected networks and discuss the difference in ability to generate synchronous spikes. Sparsely connected networks of the associative memory constructed of the binary neurons have been intensively researched (Willshaw *et al.*1969; Palm 1980; Golomb and Sompolinsky, 1990; Meunier *et al.*, 1988; Amari, 1989; Okada, 1996). However, the dynamics of associative feedforward networks constructed of spiking neurons have not.

I describe the activity in single-pattern activation in Section 4.2 and that in two-pattern activation in Section 4.3. For the latter, I described the network activity in response to the activation of two patterns with different strengths with the same timing (Subsection 4.3.1) and with the same strength but with different timings (Subsection 4.3.2). The basin of attraction is also

described in Section 4.3.3. Section 4.4 is devoted to the memory capacity of the network. Section 4.5 is a summary and discussion of this chapter.

4.2 Activation of single memory pattern

I showed that an activation similar to a memory pattern causes the propagation of the activated memory pattern with the pattern rate $F = 0.5$ in the previous chapter. In this section, I address whether the activity of the network observed by activation of one memory pattern is the same or not with the pattern rate $F \neq 0.5$.

The initial condition is the stationary distribution for no external input. For the first layer activation, we define the activity of the virtual layer (layer 0). The temporal evolution of the overlap of the first memory pattern on the virtual layer is described as the Gaussian function with standard deviation σ and total volume m^1. The volumes of the other memory patterns are set to 0. Here, the standard deviation σ is always 0.5 ms.

$$m^{0,\mu}(t) = \begin{cases} \dfrac{m^1}{\sqrt{2\pi}\sigma} \exp\left(\dfrac{(t-t_0)^2}{2\sigma^2}\right) & \mu = 1, \\ 0 & \mu \neq 1. \end{cases} \tag{4.1}$$

First, we simulated the membrane dynamics of LIF neurons as well as Chapter 3. We calculate the input currents to neurons from equations (2.4) and (2.7), membrane potential dynamics and firings from equation (2.3), and the overlaps from equation (2.6). Dashed lines in Figure 3.1 show the firing rates of neurons whose first memory pattern $\xi_i^{l,1}$ is +1. Seven layers are vertically aligned from top to bottom. Figure 3.1(a) is the case of a sparsely connected network $F = 0.4$, Figure 3.1(b) is the case of a conventional network $F = 0.5$, and Figure 3.1(c) is the case of a densely connected network $F = 0.6$. Synchronous spikes propagate in not only the case $F = 0.5$ but also $F = 0.4$ and 0.6.

Next, we apply the Fokker-Planck method. In activation of one memory pattern, it is enough to calculate 2 sublattices as well as the previous chap-

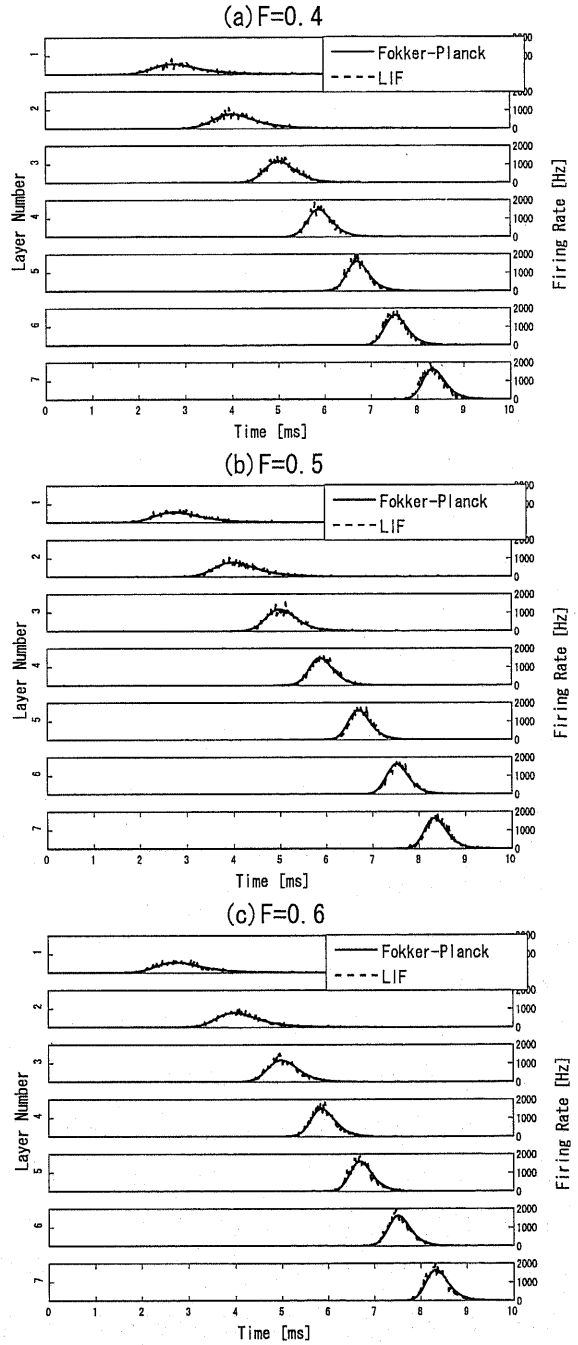
(a) F=0.4
(b) F=0.5
(c) F=0.6
Fokker-Planck
LIF
Layer Number
Firing Rate [Hz]
Time [ms]

Figure 4.1: Firing rates of the neurons whose memory pattern 1 ($\xi_i^{l,1}$) is 1 on the vertical layer following the activation of single memory pattern. The pattern rate is $F = 0.4$(a), $F = 0.5$(b), and $F = 0.6$(c). The total volume of input m^1 is 0.6. The dashed lines are obtained with the LIF simulation and the solid lines with the Fokker-Planck method. We define t^0, when $m^{0,1}(t)$ takes a peak value, as $3\sigma = 1.5$[ms].

ter. We call the sublattices (+) and (−) and calculate the distribution of membrane potential, $P_+^l(v,t)$ and $P_-^l(v,t)$, and firing rates $\nu_+^l(t)$ and $\nu_-^l(t)$ on each layer. We calculate the input current to the neurons belonging to each sublattice from equations (2.12) and (2.13), the membrane potential distributions from equation (2.9), the firing rates from equation (2.10), and the overlaps from equation (2.14). Solid lines in Figure 4.1 shows the firing rates of $\boldsymbol{\xi} = (+1)$, $\nu_+^l(t)$ on the seven layers vertically.

Figure 4.1 suggests that regardless of pattern rate F in the associative feedforward network, the spikes of the activated memory pattern synchronously propagate by one pattern activation. The results seems reasonable because equation (2.7) shows input currents to the neurons belonging the (+) sublattice do not depend on the pattern rate F. This independence from the pattern rate can be observed in the spontaneous firing modes (Figures 4.2).

Figure 4.1 also shows the consistency between the results of the LIF simulation and those of the Fokker-Planck method.

4.3 Activation of two memory patterns

In Section 3.3, I described the activities of the network by the activation of two patterns. In the analysis, I showed that an associative feedforward network has non-embedded pattern propagation mode: mixed pattern propagation mode and split propagation mode. In this section, I describe the activities by the two-pattern activation with pattern rate $F \neq 0.5$, especially the activity of the split propagation mode. As well as Section 3.3, I denote

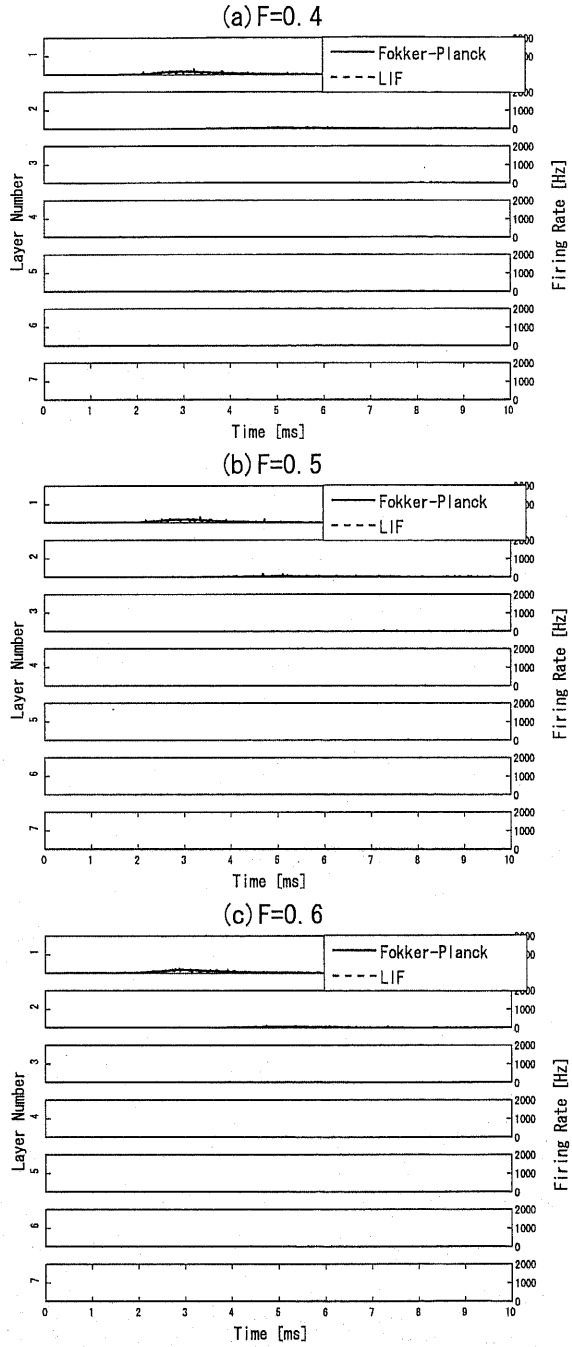
(a) F=0.4
(b) F=0.5
(c) F=0.6
Fokker-Planck
LIF
Layer Number
Firing Rate [Hz]
Time [ms]

Figure 4.2: Firing rates of the neurons whose memory pattern 1 ($\xi_i^{l,1}$) is 1 on the vertical layer under the activation of single pattern. The pattern rate is $F = 0.4$(a), $F = 0.5$(b), and $F = 0.6$(c). The total volume of input m^1 is 0.4. The dashed lines are obtained with the LIF simulation and the solid lines with the Fokker-Planck method. We define t^0, when $m^{0,1}(t)$ takes a peak value, as $3\sigma = 1.5$[ms].

the focused sublattices as $(++)$, $(+-)$, $(-+)$, and $(--)$. Accordingly the distributions of the membrane potential are described as $P^l_{++}(v,t)$, $P^l_{+-}(v,t)$, $P^l_{-+}(v,t)$, and $P^l_{--}(v,t)$, and the firing rates are $\nu^l_{++}(t)$, $\nu^l_{+-}(t)$, $\nu^l_{-+}(t)$, and $\nu^l_{--}(t)$ in layer l.

In this section, we consider the following overlaps as the activation from the virtual layer.

$$m^{0,1}(t) = \frac{1}{\sqrt{2\pi}\sigma}\left(I^0_{++}F\exp\left(\frac{(t-t_{++})^2}{2\sigma^2}\right) + I^0_{+-}(1-F)\exp\left(\frac{(t-t_{+-})^2}{2\sigma^2}\right)\right), \tag{4.2}$$

$$m^{0,2}(t) = \frac{1-F}{\sqrt{2\pi}\sigma}\left(I^0_{++}\exp\left(\frac{(t-t_{++})^2}{2\sigma^2}\right) - I^0_{+-}\exp\left(\frac{(t-t_{+-})^2}{2\sigma^2}\right)\right), \tag{4.3}$$

$$m^{0,\mu}(t) = 0 \qquad \mu \neq 1, 2. \tag{4.4}$$

Then from equation (2.13) the input to $(++)$ and $(+-)$ sublattices on the first layer is simply described as follows,

$$I^1_{++}(t) = \frac{I^0_{++}}{\sqrt{2\pi}\sigma}\exp\left(\frac{(t-t_{++})^2}{2\sigma^2}\right), \tag{4.5}$$

$$I^1_{+-}(t) = \frac{I^0_{--}}{\sqrt{2\pi}\sigma}\exp\left(\frac{(t-t_{+-})^2}{2\sigma^2}\right). \tag{4.6}$$

In Section 4.3 the results of the LIF simulation are not shown but we confirmed that their results are consistent with those of the Fokker-Planck method.

4.3.1 Activation of different input strengths

In this subsection we consider the situation where the volume of the overlaps of the two activated memory patterns on the virtual layer are respectively set to m^1 and m^2, and the timings of input to $(++)$ and $(+-)$ are set to the same value: $I^0_{++}F + I^0_{+-}(1-F) = m^1$, $(1-F)(I^0_{++} - I^0_{+-}) = m^2$, and $t_{++} = t_{+-} = t_0$ in equations (4.2) and (4.3). Therefore equations (4.5) and (4.6) are rewritten as

$$m^{0,1}(t) = \frac{m^1}{\sqrt{2\pi}\sigma} \exp\left(\frac{(t-t_0)^2}{2\sigma^2}\right), \tag{4.7}$$

$$m^{0,2}(t) = \frac{m^2}{\sqrt{2\pi}\sigma} \exp\left(\frac{(t-t_0)^2}{2\sigma^2}\right). \tag{4.8}$$

$$\tag{4.9}$$

These equations are equivalent to equation (3.2). And equations (4.5) and (4.6) are rewritten as

$$I^1_{++}(t) = \frac{m^1 + m^2}{\sqrt{2\pi}\sigma} \exp\left(\frac{(t-t_0)^2}{2\sigma^2}\right), \tag{4.10}$$

$$I^1_{+-}(t) = \frac{(1-F)m^1 - Fm^2}{(1-F)\sqrt{2\pi}\sigma} \exp\left(\frac{(t-t_0)^2}{2\sigma^2}\right). \tag{4.11}$$

Here we focus on the case that the input is similar to the first memory pattern; $m^1 \sim 1$ and $m^2 \sim 0$. If $m^2 = 0$, the input to $(++)$ and $(+-)$ sublattices is the same, $I^l_{++}(t) = I^l_{+-}(t)$ and then the memory pattern 1 propagates in the shape of synchronous firing packet as shown in Section 4.2 (Figure 4.1). We calculate in the case of $m^1 = 0.9$, $m^2 = 0.1$ by using the Fokker-Planck method. Figure 4.3 shows the firing rates $\nu^l_\xi(t)$. Solid lines indicate the firing rates of $(++)$ sublattices $\nu^l_{++}(t)$ and dashed lines are for the firing rates of $(+-)$ sublattices $\nu^l_{+-}(t)$. The pattern rate is $F = 0.4$ (Figure 4.3(a)), $F = 0.5$ (Figure 4.3(b)), and $F = 0.6$ (Figure 4.3(c)). With the pattern rate $F = 0.5$ (Figure 4.3(b)) the spikes of $(++)$ and $(+-)$ sublattices propagates in different timings. This is the split propagation mode I described in

Subsection 3.3.1. With the pattern rate $F = 0.4$ (Figure 4.3(a)), at the beginning, the neurons of $(++)$ and $(+-)$ sublattices fires in different timings but after propagation of several layers they become to fire synchronously. On the contrary, with the pattern rate $F = 0.6$, the timing difference between $(++)$ and $(+-)$ sublattices becomes larger as spikes propagate.

These results imply that in the network of the pattern rate $F < 0.5$, a sparsely connected network, synchronous firing between sublattices is promoted and in that of $F > 0.5$, a densely connected network, synchronous firing is suppressed.

The cause of these promotion and suppression of synchronous firing can be understood from the input currents to each sublattice $I^l_\xi(t)$. The input currents are described as follows:

$$
\begin{aligned}
I^{l+1}_{++}(t) &= m^{1,l}(t) + m^{2,l}(t) && (4.12)\\
&= 2F\nu^l_{++}(t) - 2(1-F)\nu^l_{--}(t) \\
&\quad + (1-2F)(\nu^l_{+-}(t) + \nu^l_{-+}(t)), && (4.13)\\
I^{l+1}_{+-}(t) &= m^{1,l}(t) - \frac{F}{1-F} m^{2,l}(t) && (4.14)\\
&= \frac{1-2F}{1-F}\left(F\nu^l_{++}(t) - (1-F)\nu^l_{--}(t)\right) \\
&\quad + \frac{2F^2 - 2F + 1}{1-F}\nu^l_{+-}(t) - 2F\nu^l_{-+}(t). && (4.15)
\end{aligned}
$$

These equations are generalized form about the pattern rate F of equations (3.3) and (3.4). With the pattern rate $F = 0.5$, that is $1 - 2F = 0$, $(++)$ sublattices do not interact with $(+-)$ as previously described. Therefore the split of spike timings caused by the difference of input strength does not change during propagation. When the pattern rate F is less than 0.5, that is $1 - 2F$ has positive value, there are excitatory connections from $(++)$ and $(+-)$ sublattices to $(+-)$ and $(++)$ sublattices in the next layer respectively. The excitatory connections promote the synchronous firing between the sublattices and finally $\nu^l_{++}(t) = \nu^l_{+-}(t)$ and $I^{l+1}_{++}(t) = I^{l+1}_{+-}(t)$ in large

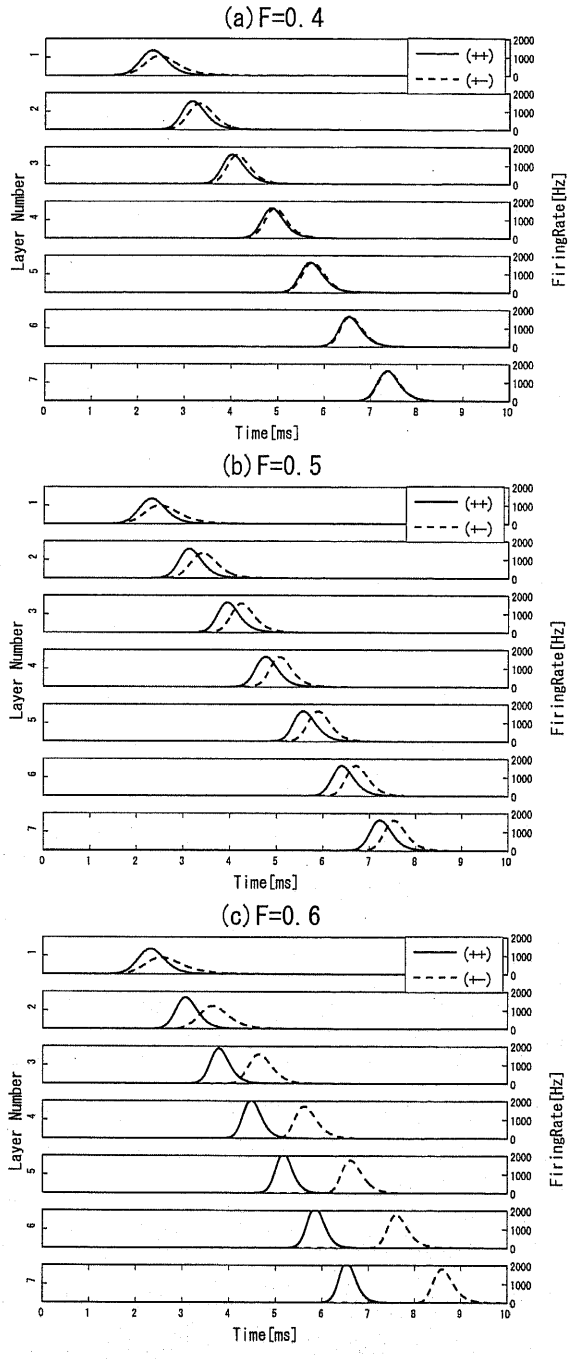
(a) F=0.4
(b) F=0.5
(c) F=0.6
(++)
(+−)
Layer Number
FiringRate[Hz]
Time[ms]

Figure 4.3: Firing rates of (++) sublattices ($\nu^l_{++}(t)$; solid lines) and (+−) sublattices ($\nu^l_{+-}(t)$; dashed lines) on the vertical layer when the strength of activation is different. The pattern rate is $F = 0.4$(a), $F = 0.5$(b), and $F = 0.6$(c). The total volume of input of the first memory pattern m^1 is 0.9 and that of the second memory pattern m^2 is 0.1. We define t^0, when $m^{0,1}(t)$ takes a peak value, as $3\sigma = 1.5$[ms]. These results is obtained with the Fokker-Planck method.

l. That is why the the split of the spike timings decreases as spikes propagate. In contrast, when the pattern rate F is more than 0.5, that is $1 - 2F$ has negative value, there are inhibitory connections as well. The inhibitory connection seems to suppress the synchronous firing and made the timing difference larger as spikes propagate.

The promotion or suppression by sparse or dense connection is regarded as disappearing or remaining of the effect of a weakly activated pattern. We can also understand this phenomena from the currents to sublattices $I^l_{\boldsymbol{\xi}}(t)$ and densities of sublattices $d(\boldsymbol{\xi})$. The densities of the (++) and (+−) sublattices are F^2 and $F(1-F)$ respectively. When the connections are sparse, (+−) has larger density and effect than (++) and *vice versa*. In addition, in the sparsely connected network the effect of pattern 2 in (+−) sublattice becomes smaller (see equation(4.14)) and that in (++) remains regardless of pattern rate (see equation(4.12)). Therefore in a sparsely connected network the effect of a weakly activated pattern becomes smaller during propagation. In contrast, in a densely connected network the effect of a weakly activated pattern remains after propagation.

4.3.2 Activation of different input timings

In the previous subsection, when the strength of input to sublattices is different, it seems that sparsely and densely connected networks respectively promote and suppress synchronous firing. To clarify whether the promotion and suppression of synchronization work by different timings activation, in

this subsection I describe the activity when we set a difference not in the strength but in the timing of input to sublattices; $I^0_{++} = I^0_{+-} = I^0$ in equations (4.5) and (4.6). Then equations (4.5) and (4.6) are rewritten as

$$I^1_{++}(t) = \frac{I^0}{\sqrt{2\pi}\sigma} \exp\left(\frac{(t-t_{++})^2}{2\sigma^2}\right), \tag{4.16}$$

$$I^1_{+-}(t) = \frac{I^0}{\sqrt{2\pi}\sigma} \exp\left(\frac{(t-t_{+-})^2}{2\sigma^2}\right). \tag{4.17}$$

We calculate in the case that the input to $(++)$ is earlier than that of $(+-)$ by 1ms, that is $t_{+-} = t_{++} + 1$[ms].

Figure 4.4 shows the firing rates $\nu^l_{\xi}(t)$. Solid lines are the firing rates of $(++)$ sublattices $\nu^l_{++}(t)$ and dashed lines are for the firing rates of $(+-)$ sublattices $\nu^l_{+-}(t)$ on the seven layers. With the pattern rate $F = 0.5$ (Figure 4.4(b)), the spikes of $(++)$ and $(+-)$ propagates at the same speed. With the pattern rate $F = 0.4$ (Figure 4.4(a)) the timing difference becomes smaller, and when the pattern rate F is 0.6 the timing difference becomes larger as spikes propagate. Figures 4.4(a-c) shows that the promotion and suppression of synchronization work under this situation. These results are consistent with the analysis of the previous subsection.

4.3.3 Basin of attraction

In Subsections 4.3.1 and 4.3.2, I showed that sparsely and densely connected networks seem to promote and suppress synchronous firing between sublattices, respectively. Here we focus on not firing timing but the stability of firing of sublattices. The timing of inputs to $(++)$ and $(+-)$ is set to be same, i.e., $t_{++} = t_{+-} = t_0$ in equations (4.5) and (4.6). Then equations (4.5) and (4.6) are rewritten as

$$I^1_{++}(t) = \frac{I^0_{++}}{\sqrt{2\pi}\sigma} \exp\left(\frac{(t-t_0)^2}{2\sigma^2}\right), \tag{4.18}$$

$$I^1_{+-}(t) = \frac{I^0_{+-}}{\sqrt{2\pi}\sigma} \exp\left(\frac{(t-t_0)^2}{2\sigma^2}\right). \tag{4.19}$$

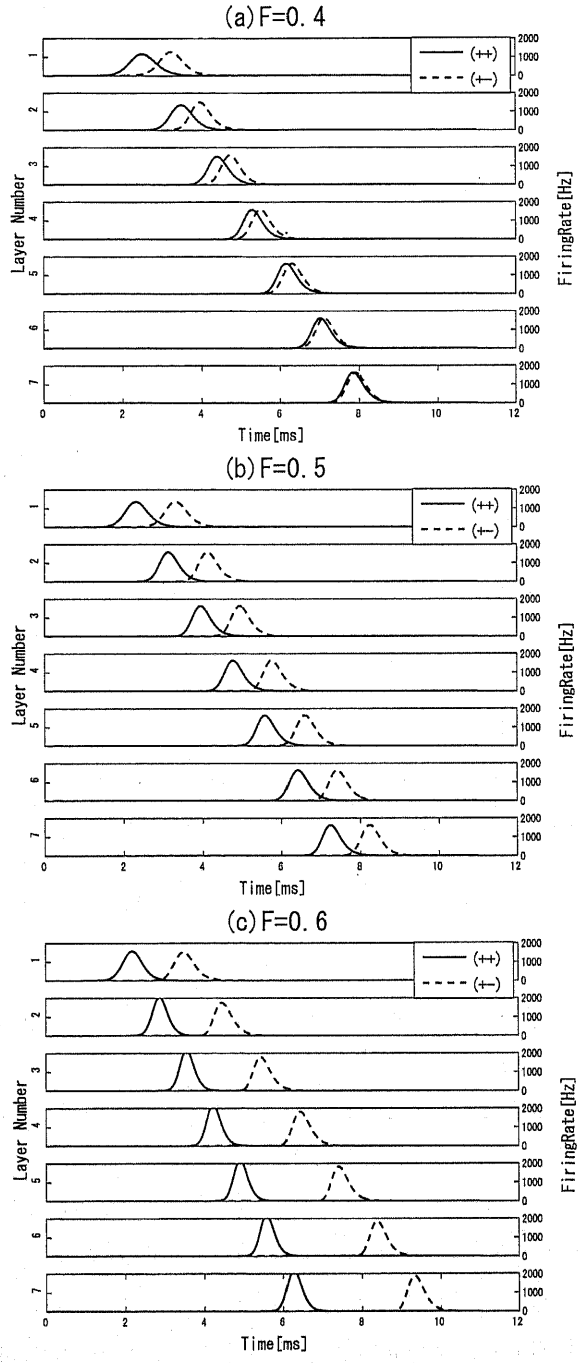
(a) F=0.4
(b) F=0.5
(c) F=0.6
(++)
(+−)
Layer Number
FiringRate[Hz]
Time[ms]

Figure 4.4: Firing rates of (++) sublattices ($\nu^l_{++}(t)$; solid lines) and (+−) ones ($\nu^l_{+-}(t)$; dashed lines) on the vertical layer when the timing of activation is different. The pattern rate is $F = 0.4$(a), $F = 0.5$(b), and $F = 0.6$(c). The size of input I^0 is 1. We define t_{++}, when $I^0_{++}(t)$ takes a peak value, as $3\sigma = 1.5$[ms] and $t_{+-} = t_{++} + 1$[ms]=2.5[ms]. These results is obtained with the Fokker-Planck method.

We observe the firing rates when we change the input strength of (++) subllatices I^0_{++} and (+−) one I^0_{+-} independently from 0 to 1. If the maximum of the firing rate of a sublattice on the fifth layer is more than 600[Hz], we regard the sublattice fires. Figure 4.5 is the result obtained with the Fokker-Planck method. The vertical axis means the input strength of (++), I^0_{++}, and the horizontal axis means that of (+−), I^0_{+-}. The black, dark gray, light gray and white region in Figure 4.5 mean no firing, activity in (++) sublattice is propagated, activity in (+−) sublattice is propagated, and memory pattern 1 is fully associated, respectively. With the pattern rate $F = 0.4$ (Figure 4.5(a)) the region of memory pattern 1 is larger than that with $F = 0.5$ (Figure 4.5(b)). In contrast, with the pattern rate $F = 0.6$ (Figure 4.5(c)) the region of memory pattern 1 is smaller than that with $F = 0.5$ (Figure 4.5(b)).

These results imply that sparsely and densely connected networks not only promote and suppress synchronous firing but also enlarge and shrink the basin of attraction of the memory pattern, respectively. The cause of enlargement and shrinkage seems to be the excitatory and inhibitory connections between sublattices as described in Subsection 4.3.1. Under the existence of excitatory connections between (++) and (+−) sublattices, (++) and (+−) sublattices mutually excite each other. On the other hand, under the existence of inhibitory connections, (++) and (+−) sublattices mutually inhibit each other and suppress the propagation.

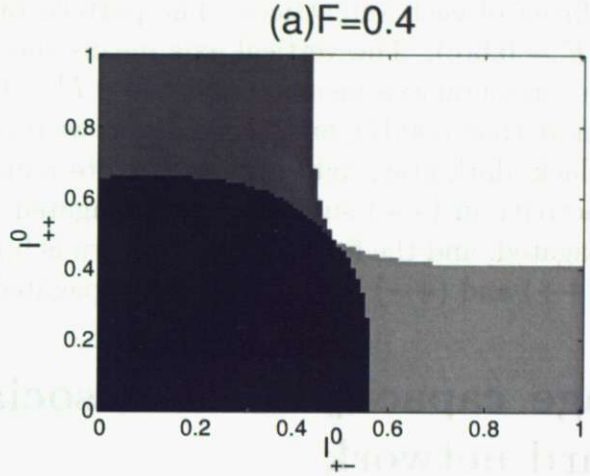
(a)F=0.4
1
0.8
0.6
0.4
0.2
0
0
0.2
0.4
0.6
0.8
1
$I^0_{\pm}$
I^0_{+-}

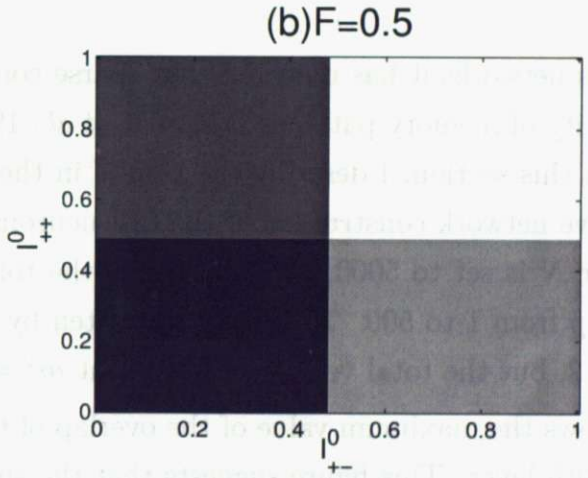
(b)F=0.5
1
0.8
0.6
0.4
0.2
0
0
0.2
0.4
0.6
0.8
1
$I^0_{\pm}$
I^0_{+-}

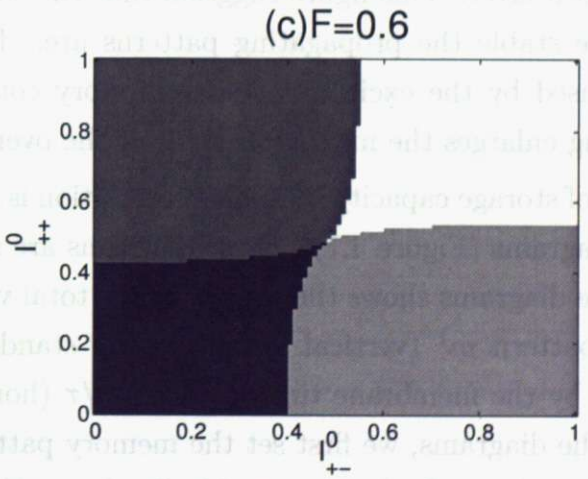
(c)F=0.6
1
0.8
0.6
0.4
0.2
0
0
0.2
0.4
0.6
0.8
1
$I^0_{\pm}$
I^0_{+-}

Figure 4.5: The firing of each sublattices. The pattern rate is $F = 0.4$(a), $F = 0.5$(b), and $F = 0.6$(c). The vertical axis means the input strength of $(++)$ I^0_{++} and the horizontal axis means that of $(+-)$ I^0_{+-}. If the maximum of the firing rate is more than 600[Hz] on the fifth layer, we regard the sublattice as 'firing'. The black, dark gray, light gray and white region in respectively mean no firing, activity in $(++)$ sublattice is propagated, activity in $(+-)$ sublattice is propagated, and the first memory pattern is fully associated and activity in both $(++)$ and $(+-)$ sublattices are propagated.

4.4 Storage capacity of an associative feedforward network

In binary neurons networks it has reported that sparse connection increases the storage capacity of memory patterns (Meunier *et al.*, 1988; Amari, 1989; Okada, 1996). In this section, I describe the results in the case of the feedforward associative network constructed of the LIF neurons. The number of neurons per layer N is set to 5000, and we change the total number of the memory pattern p from 1 to 500. The input is written by equation (4.1) as well as Section 4.2, but the total volume of the input $m^1 = 1$.

Figure 4.6 shows the maximum value of the overlap of the input memory pattern on the 20th layer. This figure suggests that the smaller the pattern rate F, the more stable the propagating patterns are. It seems that the result is also caused by the excitatory and inhibitory connections because synchronous firing enlarges the maximum value of the overlap.

The increase of storage capacity by sparse connection is also shown by the following flow diagrams (Figure 4.7). These diagrams are same diagrams as Figure 3.2. These diagrams shows the change of the total volume of overlaps of the inputed pattern m^1 (vertical axis) and the standard deviations of overlaps divided by the membrane time constant σ/τ (horizontal axis) in a layer. To draw the diagrams, we first set the memory pattern of the virtual layer $\xi_i^{0,\mu}$ as well as those of other layers. Ideally the overlap of the memory

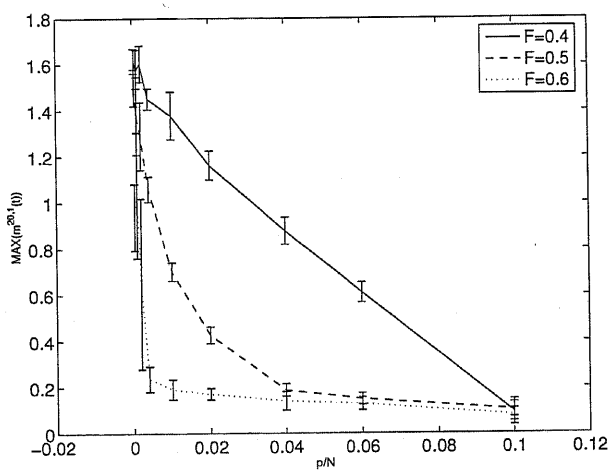

Figure 4.6: The maximum value of the overlap of the input memory pattern on the 20th layer. The horizontal axis means the rate of the total number of memory pattern p to the number of the neurons per layer N. We averaged the overlap over 10 trials and shows the standard deviations as the error-bars.

pattern 1 in the virtual layer $M^{0,1}(t)$ is the following equation;

$$M^{0,1} = \frac{m^1}{\sqrt{2\pi}\sigma} \exp\left(\frac{(t-t_0)^2}{2\sigma^2}\right). \tag{4.20}$$

In order to realize this overlap, the neurons of the virtual layer fires with the probability of $\xi_i^{0,1} M^{0,1} dt$ during time dt. We calculate the overlaps in the virtual layer not only of the memory pattern 1 but also of the other patterns from equation (2.6). Then we can calculate the input currents to the neurons in the first layer. We observed the spikes in the first layer and approximate the overlap of memory pattern 1 with the Gaussian function by using the method of least squares. Figure 4.7 shows the change of overlap between the virtual layer and the first layer. We show the change by the normalized vector from input $(m^1, \sigma/\tau)$ to the output of the overlap of memory pattern 1. Figures 4.7(a)(b) show that when the number of patterns $p = 1$, the change of overlap are independent on pattern rates F because we set the input currents independent to pattern rates (see equation (2.7)). This is also

the case of the Fokker-Planck method (data not shown). On the other hand, when the number of patterns is increased to $p = 100$ (Figures 4.7(c)(d)), the flow attracts to smaller volume in the $F = 0.6$ than $F = 0.4$. This shows the increase of storage capacity by sparse connection. This seems also the result of the noise from the excitatory(inhibitory) effects from the other memory patterns discussed Subsection 4.3.1 because the stochastic spikes in the virtual layer results in non-zero overlaps of the other memory patterns.

4.5 Summary and discussion

In this chapter, I described the activity of an associative feedforward network constructed of the LIF neurons, taking into account the sparseness of the memory patterns. The effect of sparseness has been studied mainly for recurrent networks constructed of binary neurons.

In Section 4.2, I showed that with activation of one memory pattern, the network propagates synchronous pulse packets regardless of the pattern rate (F). This is explained by the independence of the input current from the pattern rate (2.7).

In Section 4.3, I discussed the split propagation mode described in Subsection 3.3.1, which is observed following the simultaneous activation of two memory patterns. When $F = 0.5$, the split of spike timings between sublattices is preserved in the split propagation mode (Subsection 3.3.1). In contrast, the split becomes smaller and converges to zero in an $F < 0.5$ network. In an $F > 0.5$ network, the split increases during propagation. That is, in two-pattern activation, sparse (dense) connection promotes (suppressed) synchrony between sublattices because of the excitatory (inhibitory) connections between sublattices arising from the pattern rate change.

In Section 4.3.3, I described the basin of attraction observed following activation of two memory patterns. Results showed that a sparsely connected network has a larger basin of attraction than a densely connected one. This

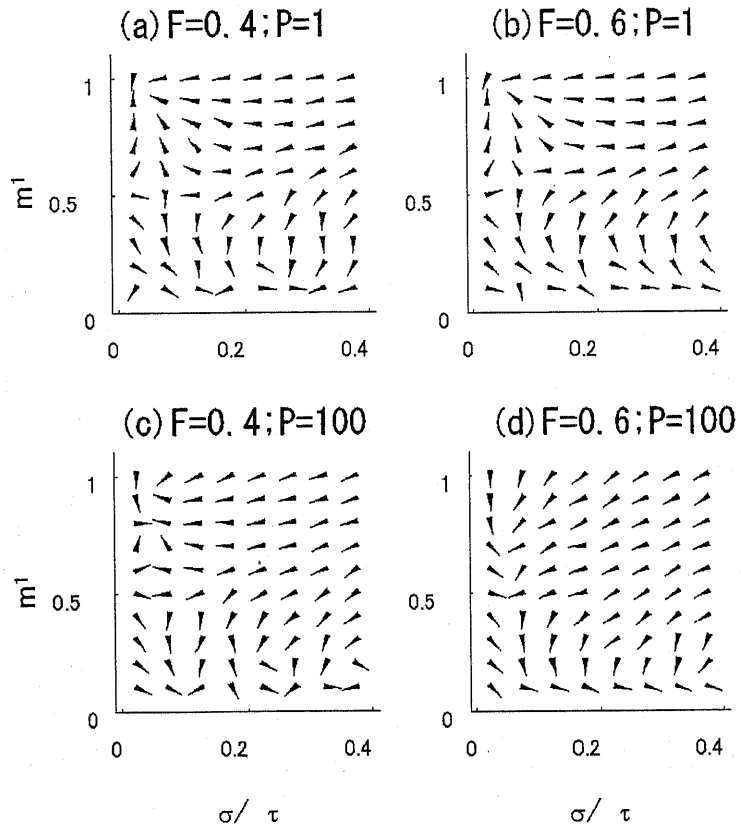

Figure 4.7: Arrows shows the change from an input overlap to an output overlap. The vertical axis means the volume of overlaps and horizontal axis means their standard deviations. The input overlaps are the Gaussian functions, and the output overlaps are approximated as the Gaussian functions. The pattern rate is $F = 0.4$ (a) and (c) and $F = 0.6$ (b) and (d). The number of embedded memory pattern is $p = 1$ (a) and (b) and $p = 100$ (c) and (d). The number of neuron is $N = 5000$.

can also be explained by the excitatory (inhibitory) connections between sublattices.

Finally, in Section 4.4, I discussed the investigation of storage capacity by using LIF simulation. The results show that a sparsely connected network has larger storage capacity than a densely connected one, corresponding to the results for recurrent networks and. The result of simulation is consistent with that of flow diagrams.

The results presented in Section 4.3.3 and Section 4.4 suggest the superiority of sparse connection for memory pattern propagation. The results presented in Section 4.3 indicate the superiority of sparse connection for synchronous firing between sublattices. However, the role of synchronous firing needs to be elucidated. Future studies will be done to clarify how neural networks can use the synchronous propagation of pulse packets for the information processing.

The question of whether sparse or dense connection is better for information processing is very important in terms of neural representation of information. It has been researched in a wide variety of fields: visual (Anderson *et al.*, 2002; Finn *et al.*, 2007), auditory (Asari *et al.*, 2006), olfactory (Wilson *et al.*, 2004; Shang *et al.*, 2007; Olsen *et al.*, 2007), and theoretical (Zhang and Sejnowski, 1999). Our results should contribute to answering the question above.

Chapter 5

Correlated memory patterns

5.1 Network model

I this dissertation, I have discussed memory patterns represented by population of neural firing and used mutually independent and orthogonalized memory patterns. However, the memory is not necessarily orthogonalized and there may be a correlation between memory patterns and concept formation (Amari, 1977). In this chapter, I discuss packet propagation when the memory patterns are correlated. For simplicity, I consider networks embedded with two correlated memory patterns.

If there is no correlation between two patterns, the density of sublattices is described by

$$\begin{aligned}&[d(++),d(+-),d(-+),d(--)]\\&\quad=[F^2,F(1-F),F(1-F),(1-F)^2],\end{aligned}\tag{5.1}$$

Here, $(++),(+-),(-+)$, and $(--)$ denotes sublattices with $(+1,+1),(+1,0),(0,+1)$, and $(0,0)$ memory patterns of a neuron $\boldsymbol{\xi}$. The correlation parameter is represented by c, and the sublattice density is given by

$$\begin{aligned}&[d(++),d(+-),d(-+),d(--)]\\&\quad=[F^2+c,F(1-F)-c,F(1-F)-c,(1-F)^2+c]\end{aligned}\tag{5.2}$$

Three constraints are placed on c because the density of sublattices must be no less than zero.

$$c \geq -F^2 \tag{5.3}$$

$$c \geq -(1-F)^2 \tag{5.4}$$

$$c \leq F(1-F) \tag{5.5}$$

We construct the associative feedforward network in accordance with the Hebbian learning rule as (equation (2.2)). Even if there is correlation between the embedded memory patterns, overlaps $m^{l,\mu}(t)$ are described by equation (2.6). By using firing rates in the layer l ($\nu^l_{++}(t), \nu^l_{+-}(t), \nu^l_{-+}(t)$, and $\nu^l_{--}(t)$), the overlaps of the two embedded patterns $(m^{1,l}, m^{2,l})$ are described by

$$m^{1,\mu}(t) = \frac{1}{F(1-F)N}\sum_{i=1}^{N}(\xi_i^{l,1} - F)\sum_{k=1}^{n}\delta(t - t^l_{i,k}). \tag{5.6}$$

$$\begin{aligned} &= \frac{1}{F(1-F)N}((F^2+c)(1-F)\nu^l_{++}(t) + ((1-F)F - c)(1-F)\nu^l_{+-} \\ &\quad - F((1-F)F - c)\nu^l_{-+} - F((1-F)^2 + c)\nu^l{--}) \end{aligned} \tag{5.7}$$

$$\begin{aligned} m^{2,\mu}(t) = &\frac{1}{F(1-F)N}((F^2+c)(1-F)\nu^l_{++}(t) - F((1-F)F - c)\nu^l_{+-} \\ &+ ((1-F)F - c)(1-F)\nu^l_{-+} - F((1-F)^2 + c)\nu^l{--}) \end{aligned} \tag{5.8}$$

From these equations, we can calculate the activity of the network using the Fokker-Planck method.

5.2 Activation of single memory pattern

In this section, I describe the activity of the network following activation of one memory pattern. For the activation, the overlaps in the virtual layer are given by

$$m^{0,\mu}(t) = \begin{cases} \dfrac{m^1}{\sqrt{2\pi}\sigma}\exp\left(\dfrac{(t-t_0)^2}{2\sigma^2}\right) & \mu = 1, \\ 0 & \mu \neq 1. \end{cases} \tag{5.9}$$

Here, $m^1 = 1$ is set to 1, which means that memory pattern 1 is strongly activated. I define $c_{MAX} \equiv F(1-F)$ for convenience.

First, I focus on a network with a pattern rate of $F = 0.5$ and calculate the network activity when $c = -c_{MAX}/4$, $-c_{MAX}/8$, 0, $c_{MAX}/8$, and $c_{MAX}/4$. Figure 5.1 shows the firing rates for the $(++)$ and $(+-)$ sublattices. The results suggest that if there is correlation, the $(++)$ and $(+-)$ sublattices do not fire synchronously. The stronger the correlation, the larger the split of spike timings. Positive (negative) correlation results in a firing order of $(++)$ then $(+-)$ ($(+-)$ and then $(++)$).

These results can be explained by the currents input to each sublattice, calculated from equation (2.13):

$$\begin{aligned} I^{l+1}_{++} &= (1-F)m^{1,l}(t) + (1-F)m^{2,l}(t) \\ &= \frac{2(F^2+c)(1-F)}{F}\nu^l_{++}(t) + \frac{(F(1-F)-c)(1-2F)}{F}(\nu^l_{+-}(t)+\nu^l_{-+}(t)) \\ &\quad - 2((1-F)^2+c)\nu^l_{--}(t), \end{aligned} \tag{5.10}$$

$$\begin{aligned} I^{l+1}_{+-} &= \frac{(F^2+c)(1-2F)}{F}\nu^l_{++}(t) + \frac{(F(1-F)-c)(2F^2-2F+1)}{F(1-F)}\nu^l_{+-}(t) \\ &\quad - 2(F(1-F)-c)\nu^l_{-+}(t) - \frac{((1-F)^2+c)(1-2F)}{1-F}\nu^l_{--}(t) \end{aligned} \tag{5.11}$$

$$\begin{aligned} I^{l+1}_{-+} &= \frac{(F^2+c)(1-2F)}{F}\nu^l_{++}(t) - 2(F(1-F)-c)\nu^l_{+-}(t) \\ &\quad + \frac{(F(1-F)-c)(2F^2-2F+1)}{F(1-F)}\nu^l_{-+}(t) - \frac{((1-F)^2+c)(1-2F)}{1-F}\nu^l_{--}(t), \end{aligned} \tag{5.12}$$

$$\begin{aligned} I^{l+1}_{--} &= 2(F^2+c)\nu^l_{++}(t) + \frac{(F(1-F)-c)(1-2F)}{1-F}(\nu^l_{+-}(t)+\nu^l_{-+}(t)) \\ &\quad - \frac{2F((1-F)^2+c)}{1-F}\nu^l_{--}(t). \end{aligned} \tag{5.13}$$

These equations mean that even if the firing of the $(++)$ and $(+-)$ sublattices are completely the same in layer l and $(-+)$ and $(--)$ do not fire ($\nu^l_{++}(t) = \nu^l_{+-}(t) = \nu(t)$ and $\nu^l_{-+}(t) = \nu^l_{--}(t) = 0$), the current input to $(++)$ and $(+-)$ sublattices in layer $l+1$ are not same when $c \neq 0$;

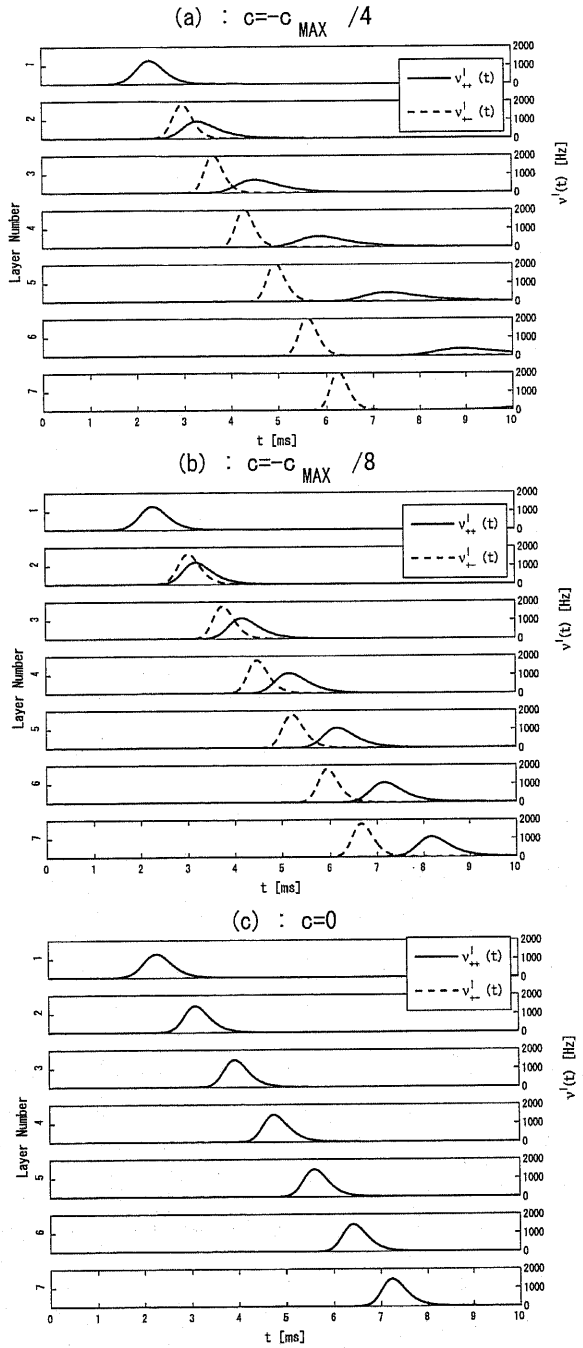
(a) : c=-c MAX /4
(b) : c=-c MAX /8
(c) : c=0
Layer Number
t [ms]
ν^l(t) [Hz]
ν^l_++ (t)
ν^l_+- (t)

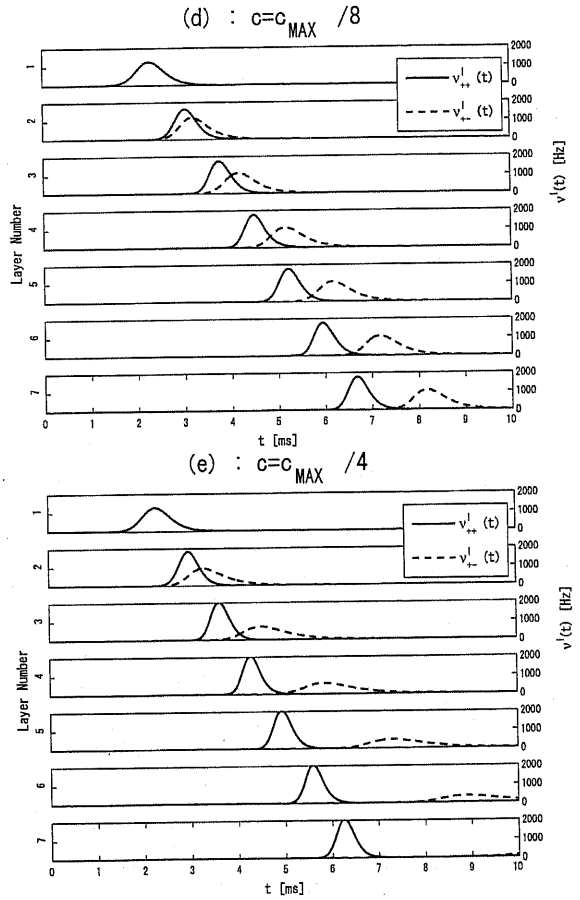

Figure 5.1: Firing rates of (++) sublattices ($\nu^l_{++}(t)$; solid lines) and (+−) ones ($\nu^l_{+-}(t)$; dashed lines) in the vertical layer obtained using Fokker-Planck method. Pattern rate F was 0.5, and correlation parameter c was (a) $-c_{MAX}/4$, (b) $-c_{MAX}/8$, (c) 0, (d)$c_{MAX}/8$, and (e) $c_{MAX}/4$. Input overlap m^1 was 1. The t_0 when $m^{0,1}(t)$ took a peak value was $3\sigma = 1.5$[ms].

$I_{++}^{l+1} - I_{--}^{l+1} = c\nu(t)/F(1-F)$. Therefore, even with the activation of one memory pattern, the spikes of $(++)$ and $(+-)$ sublattices do not synchronize (Figure 5.1).

Next, I describe the dependence on the pattern rates F under weak correlation $c = c_{MAX}/8$. As shown in Figure 5.2(a), a sparsely connected network promotes synchronous firing between sublattices in comparison to a half-connected network (Figure 5.2(b)). In contrast, as shown in Figure 5.2(c)), a densely connected network suppresses the synchronous firing and the split of the spike timings increases during propagation (Figure 5.2(c)). This dependence of synchrony on pattern rates are similar to that described in the previous chapter. The reason of the dependence is apparently the excitatory (inhibitory) connection between the different sublattices arising from sparse (dense) connection.

5.3 Summary and discussion

In this chapter, I described signal propagation when embedded memory patterns are correlated. When I embed two correlated patterns, even by single-pattern activation, the activated memory patterns do not propagate synchronously. The split is observed whether the correlation is positive or negative. This implies that correlation between memory patterns does not promote synchronous propagation and work well for synchronous signal propagation.

Moreover, sparse connection promotes synchrony and dense connection suppress it with single-pattern activation. This means that sparse connection can suppress synchrony collapse caused by pattern correlation. This also indicates the advantage of sparse connection in terms of information processing.

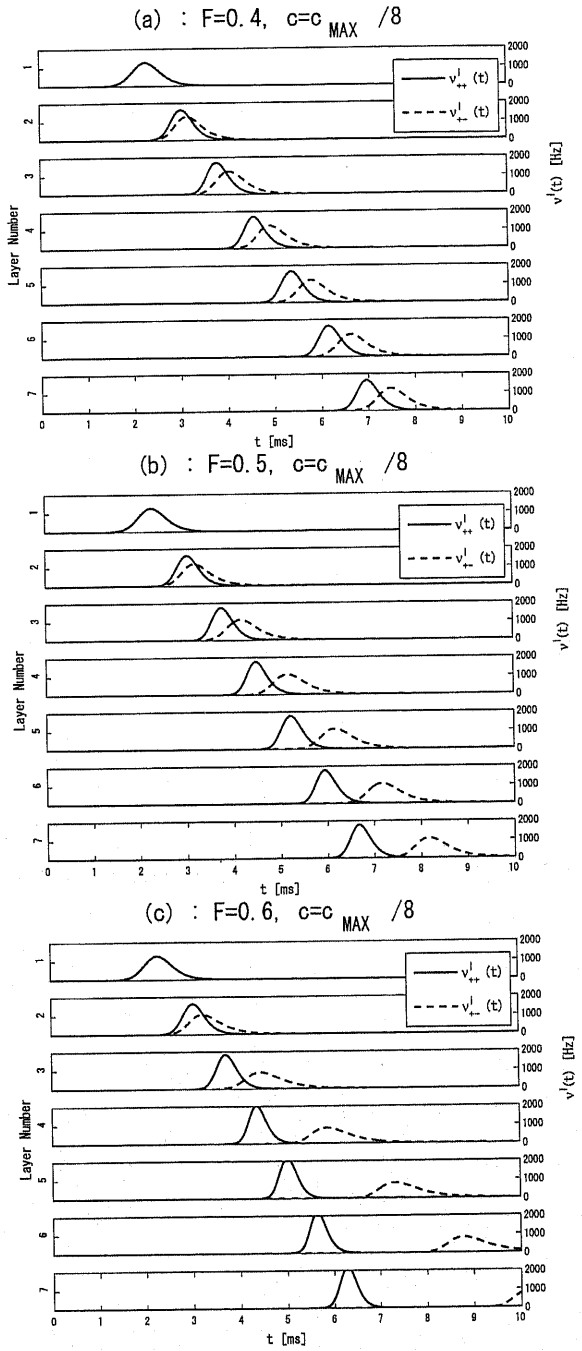
(a) : F=0.4, c=c MAX /8
(b) : F=0.5, c=c MAX /8
(c) : F=0.6, c=c MAX /8
Layer Number
t [ms]
ν^l(t) [Hz]
ν^l++ (t)
ν^l+- (t)

Figure 5.2: Firing rates of (++) sublattices ($\nu^l_{++}(t)$; solid lines) and (+−) ones ($\nu^l_{+-}(t)$; dashed lines) in the vertical layer obtained using Fokker-Planck method. Pattern rate F was (a) 0.4, (b)0.5, (c)0.6 and Correlation parameter c was $c_{MAX}/8$. Input overlap m^1 was 1. The t_0 when $m^{0,1}(t)$ took a peak value was $3\sigma = 1.5$[ms].

Chapter 6

Conclusion

6.1 Summary

In this dissertation, I described signal propagation in an associative feedforward network constructed of the LIF neurons and the analysis of its activity by using the Fokker-Planck method.

In Chapter 2, I described in detail the properties of our feedforward network. We constructed the network of LIF neurons with white Gaussian noise input. The feedforward connections are defined by the Hebbian learning rule. We were able to calculate the properties of the network without having to calculate the membrane potentials of each neurons by using the Fokker-Planck method. We described the network properties by only macroscopic parameters: $m^{l,\mu}(t)$, $P^l_{\boldsymbol{\xi}}(v,t)$, and $\nu^l_{\boldsymbol{\xi}}(t)$.

In Chapter 3, I discussed the case of pattern rate $F = 0.5$, and described three notable features. One is that the associative feedforward network can transmit an embedded memory pattern as a pulse packet as well as a homogeneous network when the network is activated by an embedded memory pattern. Another is that activation of two memory patterns produces a mixed pattern propagation mode and a split propagation mode in addition to the embedded pattern propagation mode and the spontaneous firing mode. In the mixed pattern mode, the propagation pattern is not embedded patterns

but a mixture of the embedded patterns. In the split propagation mode, the propagation pattern is an embedded pattern, but the firing is not synchronous – the propagation is split into sublattices. The last feature is that when the network is activated successively by two different patterns, the following patterns do not always propagate synchronously. They sometimes converge resulting in the split propagation mode, mixed pattern propagation mode, or the spontaneous firing mode.

In Chapter 4, I discussed the case of pattern rate is not 0.5. I described the dependence of the activity on the pattern rate (F). The activity observed following the activation of one memory pattern does not change with the pattern rate. In contrast, in the split propagation mode observed following the activation of two memory patterns, the activity changes with the pattern rate. In a sparsely connected ($F < 0.5$) network, the split of spike timing between sublattices converges to zero after propagation, and the embedded memory pattern synchronously propagates. In contrast, in a densely connected ($F > 0.5$) network, the split increases during propagation.

In addition to the split propagation mode, we analyzed the basin of attraction and storage capacity. For both, our analysis suggests that a sparsely connected network is better than a densely connected network.

In Chapter 5, I discussed the case of the correlated patterns. When correlated memory patterns are embedded, even single-pattern activation results in the split of spike timings between sublattices. This might be a disadvantage of correlated memory patterns in terms of synchronous signal propagation. Even with correlated patterns, sparse connection promotes synchronous firing and dense connection suppress. Sparse connection is thus also better in terms of synchronous signal propagation.

Our analysis of the activity of the associative feedforward network has clarified many of the properties of its propagation modes. Our research is a basic study of a network that can transmit multiple patterns of packets.

6.2 Future direction

Our research can serve as the basis for several types of studies.

One possible study is the usability of the synchrony of neural spikes, which is potentially of great benefit. As described in Chapter 1, synchronous spikes apparently play a special role in neural information processing, especially in terms of binding problem (Gray *et al.*, 1989; Gray, 1999; Singer, 1999, Engel *et al.*, 2001). Several questions, however, need to be answered: what kinds of networks generate synchronous spikes, what stimuli caused synchronous spikes, and what information do synchronous spikes transmit? Our research would help in answering the first question.

Another possible study is the construction of synfire chains using various kinds of neural models: conductance-based models, bursting neuron models, and compartment neuron models (Koch, 1999; Koch and Segev, 2001; Kistler and Gerstner, 2002; Izhikevich, 2002; Li and Greenside, 2006; Jin *et al.*, 2007). The different models result in qualitatively different changes in network activity and signal propagation. Shinozaki *et al.* reported that enhancement of pulse packet propagation by an inhibitory synaptic current can be observed in the Hodgkin-Huxley network, but not in the LIF network (Shinozaki *et al.*, 2007). Izhikevich reported that when he took account of the length of axons, the network could reproduce accurate spike trains without synchronization; he called this network activity 'polychronous' (Izhikevich, 2006). Further study using various neuron models in synfire chains or associative feedforward networks would be rewarding.

The robustness of signal propagation in the presence of various kinds of noise can be investigated. Many researches on synfire chains, including this dissertation, considered noise generated by the input current as white Gaussian noise (Diesmann *et al.*, 1999; Câteau and Fukai, 2001; Hamaguchi *et al.*, 2007; Ishibashi *et al.*, 2006; 2007). However, noise can also be expressed in the synaptic weights, or by a deficiency of neurons. Investigating this in detail is important because the robustness of pulse packet propagation is an

important feature of the synfire chain.

Our research provides useful insights for not only signal propagation but also for information representation, especially into the effect of firing sparseness. The density of spikes and the broadness of the receptive field have been hot topics in neural coding (Zhang and Sejnowski, 1999; Anderson *et al.*, 2002; Wilson *et al.*, 2004; Asari *et al.*, 2006; Finn *et al.*, 2007; Shang *et al.*, 2007; Olsen *et al.*, 2007). Our research results indicate that sparse connection is better for synchronous signal propagation.

Appendix A

Stationary membrane potential distribution and spontaneous firing rate

The initial condition for the membrane potential distribution is the stationary distribution for no synaptic current, $I_{\boldsymbol{\xi}}^{l}(t) = I_{\boldsymbol{\xi}}^{l,\alpha}(t) = 0$. The stationary distribution under the dynamics of equations (2.9) and (2.10) is obtained as follows:

$$P_{st}(v) = \frac{\nu_0}{D} \exp\left(-\frac{(v-v_0)^2}{2\tau D}\right) \int_v^{V_{th}} \Theta(u - V_{reset}) \exp\left(\frac{(u-v_0)^2}{2\tau D}\right) du, \tag{A.1}$$

where $\Theta(x)$ denotes the Heaviside function, $\Theta(x) = 1$ for $x > 0$ and $\Theta(x) = 0$ otherwise, $v_0 = V_{rest} + \tau I_0/C$, and ν_0 is the spontaneous firing rate for no synaptic current (Brunel, 2000; Hamaguchi *et al.*, 2007). $P_{st}(v)$ is the probabilistic distribution, therefore it satisfy the following normalization condition,

$$\int_{-\infty}^{V_{th}} P_{st}(v)\, dv + \tau_{ref}\nu_0 = 1, \tag{A.2}$$

where τ_{ref} is the absolute refractory period. From equation (A.2), I can get ν_0,

$$\frac{1}{\nu_0} = \tau_{ref} + \frac{1}{D}\int_{V_{reset}-v_0}^{V_{th}-v_0} du\, \exp\left(\frac{u^2}{2\tau D}\right)\int_{-\infty}^{u} dv \exp\left(-\frac{v^2}{2\tau D}\right) \tag{A.3}$$

$$= \tau_{ref} + 2\tau\sqrt{\pi}\int_{\frac{V_{reset}-v_0}{\sqrt{2\tau D}}}^{\frac{V_{th}-v_0}{\sqrt{2\tau D}}} du\, \exp(u^2)(1+\mathrm{erf}(u)), \tag{A.4}$$

where $\mathrm{erf}(x)$ is the error function, $\mathrm{erf}(x) = \frac{2}{\sqrt{\pi}}\int_0^x \exp(-y^2)dy$.

Appendix B

features of homogeneous synfire chain

A homogenous synfire chain has important features and therefore researchers have investigated the dynamics of its activities. In this chapter, I review 2 features, reproductivity and synchrony.

In this chapter, I discuss the homogeneous network and therefore synaptic weight takes same value in the network.

$$J = \frac{1}{N}. \tag{B.1}$$

Synaptic current is derived from the sum of synaptic weights in which neurons fire,

$$I^l(t) = \sum_{j=1}^{N} J \sum_{k=1}^{n} \delta(t - t_{j,k}^{l-1}) \tag{B.2}$$

$$= \frac{1}{N} \sum_{j=1}^{N} \sum_{k=1}^{n} \delta(t - t_{j,k}^{l-1}) \tag{B.3}$$

In homogeneous network, the current is firing rates of the previous layer and takes same value in one layer. Thus we can assume the current as overlap function of the previous layer. Other conditions of the network and dynamics of neurons is same as the associative feedforward network.

B.1 Reproductivity of spikes

The most important feature of a synfire chain is accurate reproductivity of spike timings. The feature enables the network to generate repeated spike patterns. What gives a synfire chain the ability? It seems the population of neurons. Figure B.1 is the raster plot of spikes of a neuron belonging to a synfire chain in 20 trials. I activate the first layer of the synfire chain by the following input:

$$I^1(t) = \frac{I_0}{\sqrt{2\pi}\sigma} \exp\left(\frac{(t-t_0)^2}{2\sigma^2}\right) \tag{B.4}$$

Figures B.1(a)-(d) means that large population of neurons can generate spikes reproducibly. Because the noise to each neuron has no correlation, the input to next layer, which is summed up the spikes, is averaged. Then if the number of neurons increases more and more, does the spike timing become more and more accurate? The reproductivity of spikes does not seem to change between the case of 100 neurons (Figure B.1(c)) and that of 1000 (Figure B.1(d)). This is because the synchrony of the spikes has deviation and the deviation depends on the convolution of α function. I review the detail about the deviation in the next section.

B.2 Synchrony of spikes

In the previous section, I showed that there are poor reproductivity in small population network, and on the other hand large population network has high reproductivity. However, these results do not mean that large population realize the synchronized firing. In fact, when the population of the neurons is small, the neurons fire synchronously. Figure B.2 shows the spikes of whole neurons in the layer 10. The vertical rows represents the trials. These figures shows that the reproductivity of the firing is different between 50 population network (Figure B.2(a)) and 1000 population network (Figure B.2(b)), and however both networks generate synchronous packet.

APPENDIX B. FEATURES OF HOMOGENEOUS SYNFIRE CHAIN

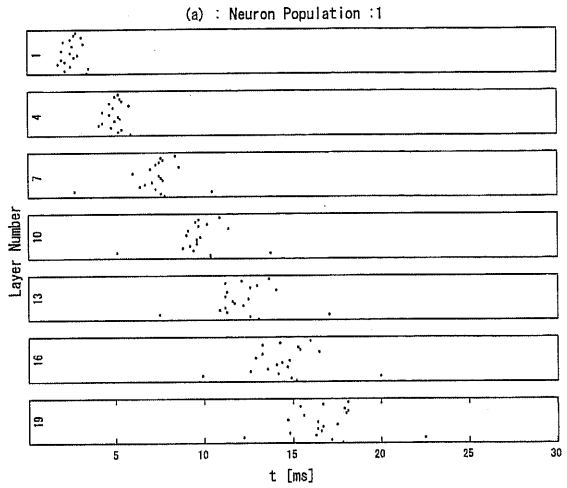

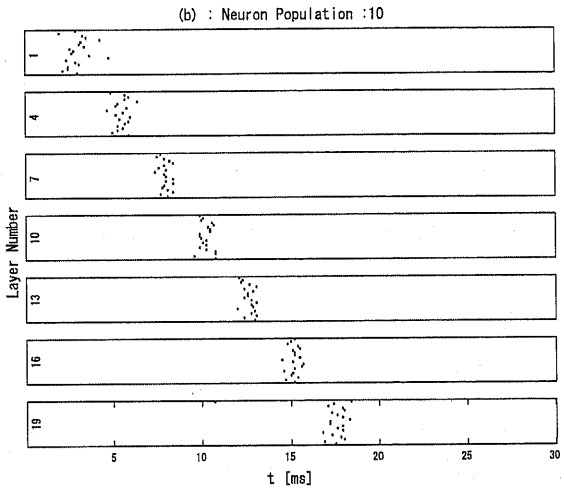

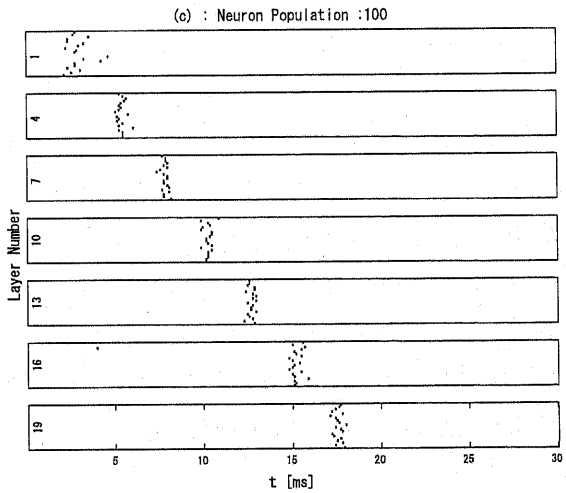

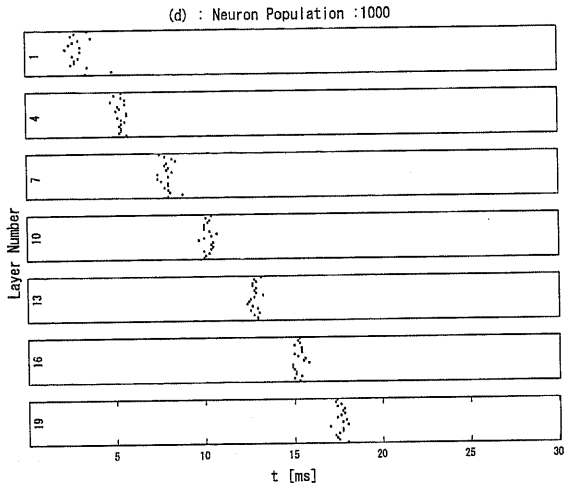

Figure B.1: Raster plots of a neuron in the vertical layer. Rows in each figure means trials. Population of neurons was (a)1, (b)10, (c)100, (d)1000. Input overlap I_0 was 0.6. The t_0 when $I^1(t)$ took a peak value was $3\sigma = 1.5$[ms].

Why do packets synchronize during propagation even in the small population network? Câteau and Fukai discussed the effect of neglecting the diffusion and relaxation during signal propagation (Câteau and Fukai, 2001). This approximation works well because the synaptic currents, $I(t)$, take much larger values than the diffusion and relaxation terms during signal propagation. By using this approximation, we can verify the reason for spike synchronization. If we neglect the diffusion and relaxation, neurons do not fire without synaptic currents. This means that the duration of output firing does not become longer than the synaptic input. Now, synaptic input is calculated from the convolution of the output firing in the previous layer and EPSP profile, α function. Figure 3.4 and B.3 supports this story. In Figure 3.4, the sharper the temporal profile of α function is, the more synchronous the attractor of the output firing is. This is consistent with the small population network (N=50) (Figure B.3).

In conclusion, the largeness of synaptic current compared to diffusion and

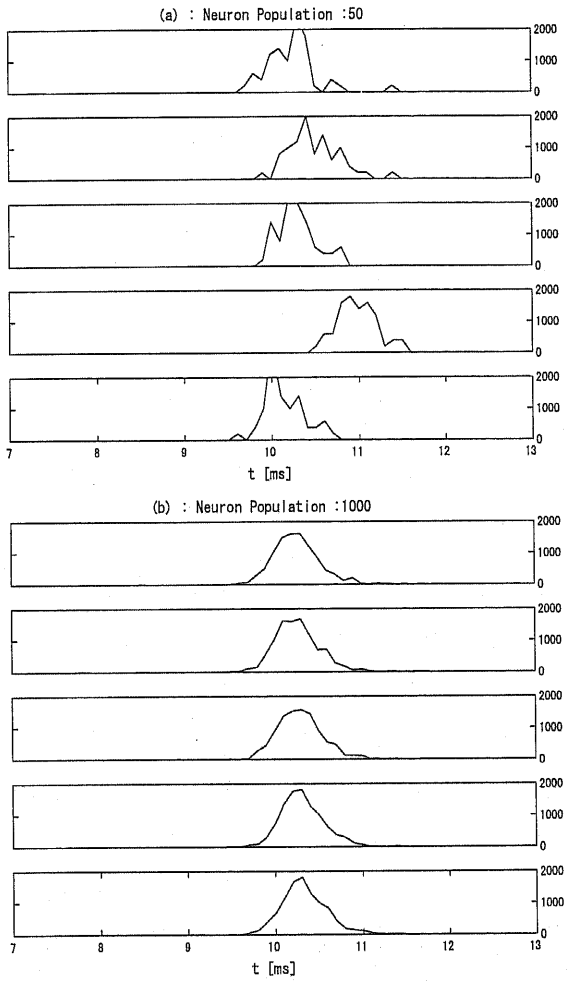

Figure B.2: Firing rates of neurons in layer 10. Vertical rows represents trials. Population of neurons was (a)50, (b)1000. Input overlap I_0 was 0.6. The t_0 when $I^1(t)$ took a peak value was $3\sigma = 1.5$[ms].

relaxation term cause the synchronous firing, regardless of the population of neurons. And the deviation of the synchrony depends on the sharpness of the temporal profile of EPSP, α function.

APPENDIX B. FEATURES OF HOMOGENEOUS SYNFIRE CHAIN

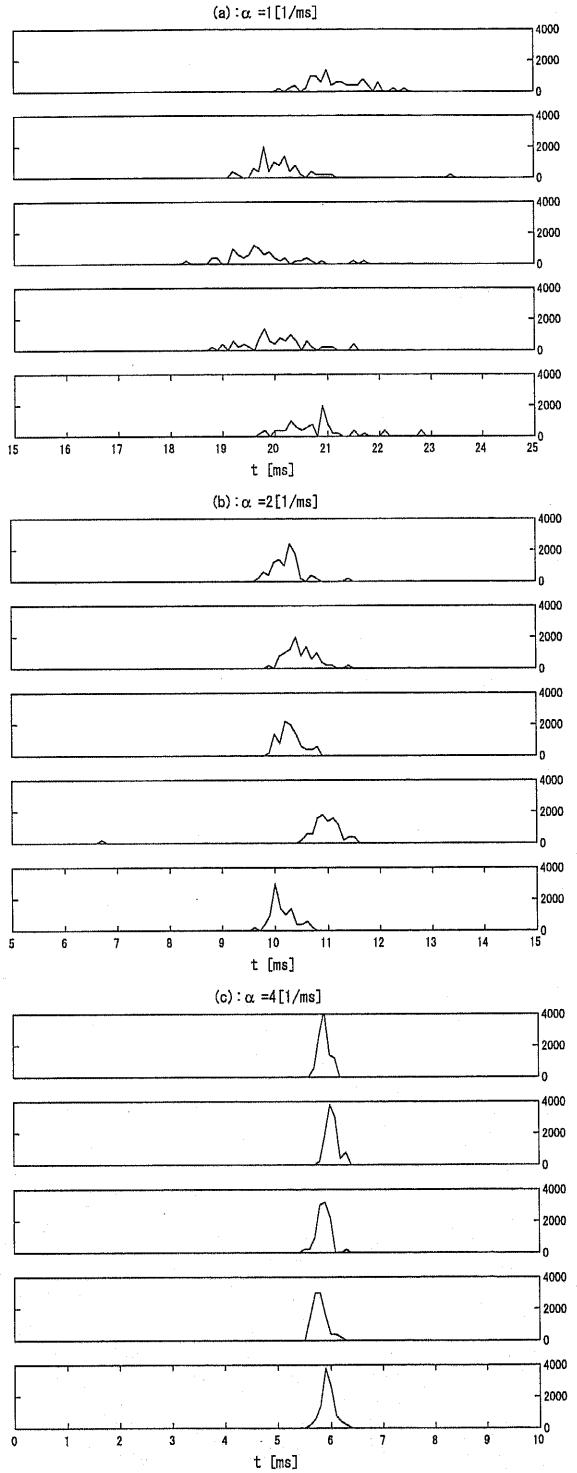

Figure B.3: Firing rates of neurons in layer 10. Vertical rows represents trials. The parameter of α function, (a)α =1ms^{-1}, (b)α =2ms^{-1}, (c)α =4ms^{-1}. Population of neurons was 50. Input overlap I_0 was 0.6. The t_0 when $I^1(t)$ took a peak value was $3\sigma = 1.5$[ms].

Bibliography

[1] Abeles, M., Gerstin, G. (1988). Detecting spatiotemporal firing patterns among simultaneously recorded single neurons. *J. Neurophysiol.* **60**, 909.

[2] Abeles, M. (1991). *Corticonics* (Cambridge: University Press).

[3] Abeles, M., Bergman, H., Margalit, E., and Vaadia, E. (1993). Spatiotemporal firing patterns in the frontal cortex of behaving monkeys. *J. Neurophysiol.* **70**, 1629.

[4] Amari, S. (1977). Neural Theory of Associative and Concept-Formation. *Biol. Cybern.* **26**, 175.

[5] Amari, S. (1989). Characteristics of sparsely encoded associative memory. *Neural Netw.* **2**, 451.

[6] Aviel, Y., Mehring, C., Abeles, M., and Horn, D. (2003). On Embedding Synfire Chains in a Balanced Network. *Neural Comp.* **15**, 1321.

[7] Amit, D. J., Gutfreund, H., and Sompolinsky, H. (1985a). Spin-glass models of neural networks., *Phys. Rev. A* **32**, 1007.

[8] Amit, D. J., Gutfreund, H., and Sompolinsky, H. (1985b). Storing Infinite Numbers of Patterns in a Spin-Glass Model of Neural Networks., *Phys. Rev. Lett.* **55**, 1530.

[9] Amit, D. J. (1989). *Modeling Brain Function* (Cambridge: University Press)

[10] Anderson, J., Lampl, I., Gillespie, D., and Ferster, D. The Contribution of Noise to Contrast Invariance of Orientation Tuning in Cat Visual Cortex. (2002). *Science* **290**, 1968.

[11] Asari, H., Pearlmutter, B., and Zador, A. (2006). Sparse Representations for the Cocktail Party Problem. *J. Neurosci.* **26**, 7477.

[12] Aviel, Y., Horn, D., and Abeles, M. (2005). Memory Capacity of Balanced Networks. *Neural Comp.* **17**, 691.

[13] Bienenstock, E. (1995). A moodel of neocortex. *Network* **6**, 179.

[14] Bienenstock, E., Cooper, L., and Munro, P. (1982). Theory for the development of neuron selectivity: orientation specificity and binocular interaction in visual cortex. *J. Neurosci.* **2**, 32.

[15] Brunel, N. (2000). Dynamics of Sparsely Connected Networks of Excitatory and Inhibitory Spiking Neurons. *J. Comput. Neurosci.* **8**, 183.

[16] Câteau, H., and Fukai, T. (2001). Fokker-Planck approach to the pulse packet propagation in synfire chain. *Neural Netw.* **14**, 675.

[17] Chang, J. S., and Cooper, G. (1970). A practical difference scheme for Fokker-Planck equations. *J. Comput. Phys.* **6**, 1.

[18] Cooper, L. N., Liberman, F., and Oja, E. (1979). A theory for the acquisition and loss of neuron specificity in visual cortex. *Biol. Cybern.* **33**, 9.

[19] Dayan, P. and Sejnowski, T. (1993). The Variance of Covariance Rules for Associative Matrix Memories and Reinforcement Learning. *Neural Comp.* **5**, 205.

[20] Diesmann, M., Gewaltig, M.-O., and Aertsen, A. (1999). Stable propagation of synchronous spiking in cortical neural networks. *Nature* **402**, 529.

[21] Domany, E. and Meir, R. (1986). Storing and retrieving information in a layered spin system. *Europhys. Lett.* **3**, 175.

[22] Engel, A. K. and Fries, P. and Singer, W. (2001). Dynamic predictions: oscillations and synchrony in top-down processing. *Nature Reviews Neurosci.* **2**, 704.

[23] Finn, I., Priebe, N., and Ferster, D. (2007). The Emergence of Contrast-Invariant Orientation Tuning in Simple Cells of Cat Visual Cortex. *Neuron* **54**, 137.

[24] Gerstner, W. and van Hemmen, J. L. (1992). Associative memory in a network of 'spiking' neurons. *Network: Computation in Neural Systems* **3**, 139.

[25] Gerstner, W. and Kistler, W. (2002). *Spiking Neuron Models: Single Neurons, Populations, Plasticity* (Cambridge: University Press)

[26] Gewaltig, M.-O., Diesmann, M., and Aeatsen, A. (2001). Propagation of cortical synfire activity: survival probability in single trials and stability in the mean. *Neural Netw.* **14**, 657.

[27] Golomb, D. and Sompolinsky, H. (1990). Willshaw model: associative memory with sparse coding and low firing rates. *Physical Review A* **41**, 1843.

[28] Gray, C. M., König, P., Engel, A. K., and Singer, W. (1989). Oscillatory responses in cat visual cortex exhibit inter-columner synchronization which reflects global stimulus properties. *Nature* **338**, 334.

[29] Gray, C. M. (1999). The Temporal Correlation Hypothesis of Visual Feature Integration: Still Alive and Well. *Neuron* **24**, 31.

[30] Hamaguchi, K., Okada, M., Kuboda, S., and Aihara, K. (2005). Stochastic resonance of localized activity driven by common noise. *Biol. Cybern.* **92**, 438.

[31] Hamaguchi, K., Okada, M., Yamana, M., and Aihara, K. (2005). Correlated Firing in a Feedforward Network with Mexican-Hat-Type Connectivity. *Neural Comp.* **17**, 2034.

[32] Hamaguchi, K., Okada, M., and Aihara, K. (2007). Variable Timescales of Repeated Spike Patterns in Synfire Chain with Mexican-Hat Connectivity. *Neural Comp.* **19**, 2468.

[33] Hahnloser, R., Kozhevnikov, A, and Fee, M. (2002). An ultra-sparse code underlies the generation of neural sequences in a songbird. *Nature* **419**, 65.

[34] Hebb, D. O. (1949). *The organization of behavior.* (New York: Wiley).

[35] Hopfield, J. J. (1982). Neural Networks and Physical Systems with Emergent Collective Computational Abilities. *Proc. Natl. Acad. Sci.* **79**, 2554.

[36] Herrmann, M., Hertz, J., and Prügel-Bennett, A., (1995). Analysis of Synfire Chains. *Network: Computation in Neural Systems* **6**, 403.

[37] Ikegaya, Y., Aaron, G., Cossart, R., Aronov, D., Lampl, I., Ferster, D., and Yuste, R. (2004). Synfire Chains and Cortical Songs: Temporal Modules of Cortical Activity. *Science* **304**, 559.

[38] Ishibashi, K., Hamaguchi, K., and Okada, M. (2006). Theory of interaction of memorya patterns in layered associative networks. *J. Phys. Soc. Jpn.* **75**, 114803.

[39] Ishibashi, K., Hamaguchi, K., and Okada, M. (2007). Sparse and Dense Encoding in Layered Associative Network of Spiking Neurons. *J. Phys. Soc. Jpn.* **76**, 124801.

[40] Izhikevich, E. M. (2002). Which Model to Use for Cortical Spiking Neurons? *IEEE Trans. Neural Netw.* **15**, 5.

[41] Izhikevich, E. M. (2006). Polychronization: computation with spikes. *Neural Comp.* **18**, 245.

[42] Jin, D. Z., Ramazanoğlu, F. M., and Seung, H. S. (2007). Intrinsic bursting enhances the robustness of a neural network model of sequence generation by avian brain area HVC. *J. Comput. Neurosci. 23*, 283.

[43] Kandel, E. R., Schwartz, J. H. and Jessell, T. M. (2000), *Principles of Neural Science* (McGraw-Hill)

[44] Kistler, W. M., and Gerstner, W. (2002). Stable Propagation of Activity Pulses in Populations of Spiking Neurons. *Neural Comp.* **14**, 987.

[45] Koch, C. (1999). *Biophysics of Computation: Information Processing in Single Neurons* (Oxford University Press).

[46] Koch, C. and Segev, I. (2001). *Methods in Neural Modeling: From Ions to Networks* (MIT Press).

[47] Li, M. R. and Greenside, H. (2006). Stable propagation of a burst through a one-dimensional homogeneous excitatory chain model of songbird nucleus HVC. *Phys. Rev. E* **74**, 11918.

[48] Mainen, Z. and Sejnowski, T. (1995). Reliability of Spikt Timing in Neocortical Neurons. *Science* **268**, 1503.

[49] Meir, R. and Domany, E. (1987). Stochastic dynamics of a layered neural network; exact solution. *Europhys. Lett.* **4**, 645.

[50] Meir, R. and Domany, E. (1987). Exact solution of a layered neural network model. *Phys. Rev. Lett.* **59**, 359.

[51] Meir, R. and Domany, E. (1988). Layered feed-forward neural network with exactly soluble dynamics. *Phys. Rev. A* **37**, 2660.

[52] Meunier, C. Yanai, H., and Amari, S. (1991). Sparsely coded associative memories: capacity and dynamical properties. *Network: Computation in Neural Systems* **2**, 469.

[53] Mokeichev, A., Okun, M., Barak, O., Katz, Y., Ben-Shahar, O., and Lampl, I. (2007). Stochastic emergence of repeating cortical motifs in spontaneous membrane potential *in vivo*. *Neuron* **53**, 413.

[54] Okada, M. (1996). Notions of Associative Memory and Sparse Coding. *Neural Netw.* **9**, 1429.

[55] Olsen, S., Bhandawat, V., and Wilson, R. (2007). Excitatory Interactions between Olfactory Processing Channels in the Drosophila Antennal Lobe. *Neuron* **54**, 89.

[56] Palm, G. (1980). On associative memory. *Biol. Cybern.* **36**, 19.

[57] Panzeri, S., Rolls, E. T., Battaglia, F., and Lavis, R. (2001). Speed of feedforward and recurrent processing in multilayer networks of integrate-and-fire neurons. *Network: Computation in Neural Systems* **12**, 423.

[58] Park, B. T., and Petrosian, V. (1996). Fokker-Planck Equations of Stochastic Acceleration: A Study of Numerical Methods. *Astrophys. J. Suppl.* **103**, 255.

[59] Prut, Y., Vaadia, E., Bergman, H., Haalman, I., Solvin, H., and Abeles, M. (1998). Spatiotemporal Structure of Cortical Activity: Properties and Behavioral Relevance. *J. Neurophysiol.* **79**, 2857. 529.

[60] Reyes, A. (2003). Synchrony-dependent propagation of firing rate in iteratively constructed networks *in vitro*. *Nature Neurosci.* **6**, 593.

[61] Risken, H. (1996). *The Fokker-Planck Equation.* (Springer).

[62] Shang, Y., Claridge-Chang, A., Sjulson, L., Pypaert, M., and Miesenböck, G. (2007). Excitatory Local Circuits and Their Implications for Olfactory Processing in the Fly Antennal Lobe. *Cell* **128**, 601.

[63] Shinozaki, T., Câteau, H., Urakubo, H., and Okada, M. (2007). Controlling Synfire Chain by Inhibitory Synaptic Input. *J. Phys. Soc. Jpn.* **76**, 044806.

[64] Shmiel, T., Drori, R., Shmiel, O., Ben-Shaul, Y., Nadasdy, Z., Shemesh, M., Teicher, M., and Abeles, M. (2005). Neurons of the cerebral cortex exhibit precise inter-spike timing in correspondence to behavior. *Proc. Natl. Acad. Sci.* **102**, 18655

[65] Shmiel, T., Drori, R., Shmiel, O., Ben-Shaul, Y., Nadasdy, Z., Shemesh, M., Teicher, M., and Abeles, M. (2005). Temporally precise cortical firing patterns are associated with distinct action segments. *J. Neurophysiol.* **96**, 2645.

[66] Singer, W. (1999). Neuronal Synchrony: A Versatile Code for the Definition of Relations? *Neuron* **24**, 49.

[67] Teramae, J. and Fukai, T. (2007). Local cortical circuit model inferred from power-law distributed neuronal avalanches. *J. Comput. Neurosci.* **22**, 301.

[68] van Rossum, M. C. W., Turrigiano, G., and Nelson, S. (2002). Fast Propagation of Firing Rates through Layered Networks of Noisy Neurons. *J. Neurosci.* **22**, 1956.

[69] Willshaw, D. J., Buneman, O. P., and Longuet-Higgins, H. C. (1969). Non-holographic associative memory. *Nature* **222**, 960.

[70] Wilson, R, Turner, G. C., and Laurent, G. (2004). Transformation of olfactory representations in the *Drosophila* antennal lobe. *Science* **303**, 366.

[71] Zhang, K. and Sejnowski, T. (1999). Neuronal tuning: to sharpen or broaden?. *Neural Comp.* **11**, 75.